

DISSERTATION

DEVELOPMENT OF A PETAWATT CLASS TI:SAPPHIRE LASER FOR THE EXCITATION
OF EXTREME RADIATION SOURCES

Submitted by

Alex Pratt Rockwood

Department of Physics

In partial fulfillment of the requirements

For the Degree of Doctor of Philosophy

Colorado State University

Fort Collins, Colorado

Spring 2020

Doctoral Committee:

Advisor: Jorge J. Rocca

Siu Au Lee

Jacob L. Roberts

Mario C. Marconi

Copyright by Alex Pratt Rockwood 2020

All Rights Reserved

ABSTRACT

DEVELOPMENT OF A PETAWATT CLASS TI:SAPPHIRE LASER FOR THE EXCITATION OF EXTREME RADIATION SOURCES

This dissertation describes the design, construction and characterization of a high peak power, high repetition rate, Titanium-Sapphire laser system. This chirped-pulse amplification (CPA) laser delivers femtosecond pulses of up to 0.85 PW peak power. By utilizing pump laser amplifiers with a slab configuration high repetition rate are achieved, 3.3Hz, the highest at which Petawatt-class lasers have been operated to date. This 800nm laser also has a high power, ultra-high contrast 400 nm beamline. By frequency doubling the 800 nm with a KDP crystal at $\geq 40\%$ conversion we are able to achieve a contrast of $> 1 \times 10^{-12}$. The ability to focus this second harmonic beam to $\sim 1.2 \mu\text{m}$ Full Width at Half Maximum (FWHM) spot size made it possible to achieve intensities up to $\sim 6.5 \times 10^{21} \text{ W/cm}^2$. With these high intensities and high contrast this laser is a powerful tool in many applications especially in the study of laser/matter interactions at relativistic plasmas.

This Ti:Sapphire laser was used for the excitation of plasma based soft x-ray (SXR) lasers. prior to this work compact, repetitively fired, gain-saturated x-ray lasers had been limited to wavelengths above $\lambda = 8.85 \text{ nm}$. We were able to demonstrate SXR lasers operating in the gain-saturated regime down to wavelengths as low as $\lambda = 6.85 \text{ nm}$ in Ni-like Gd. Gain was also observed at $\lambda = 6.4 \text{ nm}$, and $\lambda = 5.8 \text{ nm}$ in Ni-like Dy. As an application of plasma-based SXR lasers, single shot Fourier holograms covering a large area of view were demonstrated using an 18.9nm laser with high spatial coherence based on dual plasma amplifier. Compact SXR lasers have made possible applications in nano-scale imaging, dense plasma diagnostics and a variety of new studies of materials and surfaces. Other applications that were enabled by this Petawatt-class laser discussed elsewhere include the study of the interaction of relativistic laser pulses

with aligned nanostructures, producing record conversion efficiency of optical laser light into picosecond x-ray pulses with photons of > 1 KeV energy and flashes of deuterium-deuterium fusion neutrons.

ACKNOWLEDGEMENTS

I would like to express my sincere gratitude to my advisor Professor Jorge Rocca for the continuous support of my Ph.D study and related research, for his patience, motivation and immense knowledge. I would like to thank him for the opportunity to work with him at Colorado State University's Engineering Research Center for Extreme Ultraviolet Science and Technology and LaserNetUS. Besides my advisor, I would like to thank the rest of my thesis committee: Professor Siu Au Lee, Professor Mario Marconi and Professor Jacob Roberts for their insightful comments and encouragement.

I would also acknowledge everyone who has helped me during my time at the laboratory; Yong Wang, Shoujun Wang, Liang Yin, Reed Hollinger, Adam Moreau, Clayton Bargsten, Alden Curtis, Chase Calvi, Brad Luther, David Alessi, Hanchen Wang, Ilya Kuznetsov, Maria Gabriela Capeluto, Li Wei, Travis Day, Tyler Green, Herman Bravo, Michael Pedicone, Han Chi, Emmett Randel, Drew Schiltz, Nils Monserud, Joe Merritt, Lukasz Urbanski, Chan Kyaw, Ray Spencer, Jeremy Andreasik, Borja Iban Gonzalez, Vyacheslav Shlyaptsev, Inigo Garavilla Adrian, Xiang Sun, Stephan Meyer, Patrick Stockton, Zackery Roberso, Cory Baumgarten, Shaun Meehan, Keith Wernsing, Joel Stewart, Jon ArreguiPeman, Jon Bailach-Arrate, Morris Schmidt, Nick Detrez, Chad Beardall, Huanyu Song, Brendan Reagan, Mike Grisham, Mark Berrill, Mark Woolston and Dinesh Patel.

Last but not the least, I would like to thank my family: My kids and my parents and to my brothers and sister and also thanks my friends for all of their love and support. Without any of these people this would not be possible.

DEDICATION

I would like to dedicate this thesis to my loving parents and family.

TABLE OF CONTENTS

ABSTRACT	ii
ACKNOWLEDGEMENTS	iv
DEDICATION	v
LIST OF FIGURES	viii
Chapter 1 Introduction	1
1.1 Petawatt-class laser systems	4
1.2 Petawatt-class Chirped Pulse Amplification Lasers	9
1.2.1 Laser Oscillator	9
1.2.2 Stretcher and Compressor	11
1.2.3 Amplification	16
1.2.4 Mitigation of parasitic lasing	18
1.3 Foreword	20
Bibliography	21
Chapter 2 0.85 PW Laser operation at 3.3 Hz and high-contrast ultrahigh-intensity $\lambda =$ 400 nm second-harmonic beamline	31
2.1 Overview	31
2.2 Development of the high peak power laser and its characteristics	31
2.3 Conclusions	40
Bibliography	41
Chapter 3 Compact gain-saturated x-ray lasers down to 6.85 nm and amplification down to 5.85 nm	46
3.1 Overview	46
3.2 Introduction	46
3.3 Experimental set up and methods	48
3.4 Results	52
3.5 Conclusion	60
Bibliography	62
Chapter 4 Single shot, large field of view, Fourier transform holography with 5 ps resolution using an 18.9 nm laser	68
4.1 Overview	68
4.2 Introduction	68
4.3 Experimental Setup	71
4.3.1 Highly coherent SXR laser	72
4.3.2 Zone Plate	75
4.3.3 Sample holder and CCD	77

4.4	Results	78
4.5	How to further improve resolution in future work	81
Bibliography	85
Chapter 5	Summary	92
Appendix A	RELATED WORK	93

LIST OF FIGURES

1.1	Illustration of a classic CPA laser system.	6
1.2	Evolution of the laser spectra through the system	7
1.3	Schematic diagram of Ti:Sapphire CPA laser system developed at CSU.	10
1.4	Schematic Diagram of the Ti:Sapphire Oscillator.	11
1.5	Schematic layout of a grating-based stretcher and schematic layout of a grating-based compressor.	12
1.6	Simulation of the folded telescope stretcher.	14
1.7	Photograph of stretcher at Colorado State University.	15
1.8	Illustration of effect of gain narrowing on spectrum and method to prevent it.	17
1.9	Illustration of Ti:Sapphire rod with ASE parasitic lasing and examples of output.	19
2.1	Diagram of 3.3 Hz, 0.85 PW CPA Ti:Sa laser system.	33
2.2	Beam output profile of 0.85PW Ti:Sa System	35
2.3	Simulation of the grating compressor at Colorado State University.	36
2.4	Photograph of grating compressor, roof mirror and turning mirror.	37
2.5	Autocorrelation trace of the compressed pulses	38
2.6	Shot-to-shot pulse energy variation of Ti:Sa laser	38
2.7	Doubling efficiency as a function of input pulse energy.	39
3.1	Solid rendering of the experimental setup for the pumping and measurement of the plasma based laser.	48
3.2	Measured temporal profile of pre-pulse laser that pumps plasma based laser.	49
3.3	Measured spectrum of Ti:Sapphire with and with-out use of AOPDF to cut bandwidth.	49
3.4	End-on spectra showing the $\lambda = 7.36$ nm	51
3.5	Measured $\lambda = 7.36$ nm laser intensity as a function of the pre-pulse duration.	52
3.6	Measured laser intensity as a function of the delay between the peak of the pre-pulse and the peak of the short pulse.	52
3.7	Intensity of the $\lambda = 7.36$ nm laser line of Ni-like Sm as a function of the plasma-column length.	53
3.8	End-on spectra of a line-focus Gd plasma column showing saturated amplification in the $\lambda = 6.85$ nm line of Ni-like Gd.	54
3.9	Intensity of the $\lambda = 6.85$ nm laser line as a function of the plasma-column length.	55
3.10	Measured and simulated Ni-like Gd laser far field beam intensity profile.	56
3.11	Computed evolution of the intensity distribution of the x-ray laser beam of the 6.85 nm line of Ni-like Gd as function of plasma column length.	57
3.12	Computed evolution of the intensity distribution of the x-ray laser beam of the 6.85 nm line of Ni-like Gd as function of plasma column length.	58
3.13	End-on spectra showing lasing at progressively shorter wavelengths.	59
3.14	Measured optimum grazing incidence angle as a function of atomic number.	59
3.15	The optimum grazing incidence angle as a function of lasing wavelength.	60

4.1	Depiction of the Fourier holography setup with zone plate and sample with the two holes followed by a CCD.	72
4.2	Depiction of the seed and amplifier setup used by Colorado State University to create spatially coherent SXR beam.	74
4.3	Dual molybdenum amplifier SXR 18.9nm beam after passing through a double slit showing interference and good spatial coherence.	75
4.4	Unseeded Ni-like Mo 18.9nm SXR laser and Ni-like Mo 18.9nm SXR laser seeded Ni-like Mo 18.9nm SXR laser in the far field.	75
4.5	Depiction of a zone plate and the different order focus and directions.	77
4.6	Electron microscope image of two samples used in this work. Each sample has a 7 μm hole with 200 nm silver nanowires over it and a 3 μm hole separated by 11 μm	79
4.7	Typical single shot SXR Fourier holography image taken with a zoom of the fringe pattern.	79
4.8	The Fourier transform of the hologram and a zoom of the section showing the sample and the 200nm silver nano-wires.	80
4.9	Electron microscope image (left) and single shot holographic images (right) of the 200 nm silver nanowires over a 7 μm hole.	81
4.10	A 10% to 90% characteristic knife edge cut of the image showing a spatial resolution of 62 nm.	82
4.11	Illustration of zone plate sag and effects on focus.	84

Chapter 1

Introduction

Petawatt-class lasers are transforming the field of high energy density physics. They transform materials into states characterized by extreme temperature, density and degree of ionization. Petawatt-class lasers They also generate extreme electromagnetic fields, that make possible a myriad of applications. These include the generation of secondary sources of high energy photons (x-rays and gamma-rays), beams of high energy electrons and ions and flashes of neutrons. They can be coupled and synchronized with other lasers, ion and electron accelerators, x-ray sources and z-pinches [1]. This dissertation presents the development of a petawatt-class laser at Colorado State University (CSU) operating at a wavelength of 800 nm. With the repetition rate of 3.3 Hz and peak power of 0.85 PW, it is currently the highest average repetition rate petawatt-class laser in the world. These laser parameters along with the ability to frequency double the pulse into a high contrast 400nm beam make it an extremely useful tool. The petawatt-class laser that is the central tool of this thesis was successfully used in several applications at CSU. These include the pumping of plasma-based soft x-ray (SXR) lasers and their application to ultrafast ultra-high resolution holography, the generation of extreme plasma conditions by irradiation of nano-wire arrays, the generation of flashes of x-rays of picosecond duration, electron/ion acceleration and neutron generation flash through deuterium-deuterium nuclear fusion. The first two applications are introduced in the following paragraphs and are discussed in detail in Chapter 3 and Chapter 4 of this dissertation.

Soft x-ray lasers:

We have extended the range of repetitively fired x-ray lasers to $\lambda = 6.85$ nm by transient traveling wave excitation of Ni-like Gd ions in a plasma created with an optimized pre-pulse followed by rapid heating with an intense sub-ps pump pulse. Isoelectronic scaling also produced strong lasing at 6.67 nm and 6.11 nm in Ni-like Tb, and amplification at 6.41 nm and 5.85 nm in

Ni-like Dy. We experimentally demonstrate that the optimum grazing incidence angle increases linearly with atomic number from 17 degrees for $Z=42$ (Mo) to 43 degrees for $Z=66$ (Dy). [2]

Single shot large field of view nano-holography:

Using a SXR laser pumped by the Ti:Sapphire laser described here in we were able to demonstrate single shot Fourier transform holography with a spacial resolution that gets to 62 nm and temporal resolution of 5 ps over a large field of view. A highly coherent Ni-like molybdenum SXR laser at 18.9 nm was used. Utilizing a dual-plasma scheme in which a small fraction of the wavefront generated from a first SXR laser plasma amplifier is injected into a second plasma amplifier we were able to achieve a high spatial coherence necessary for holography. silver nano-wires 200 nm in diameter were imaged over a $7 \mu\text{m}$ diameter field of view utilizing a reference beam focused through a $3 \mu\text{m}$ hole by a 200 nm outer zone free standing zone plate (ZP). The final acquired image was numerically reconstructed by 2D Fourier transform. The 10%– 90% knife edge spatial resolution was measured with the best value reaching down to 62 nm.

Other applications of this Petawatt-class laser realized with the contribution of this author are outlined below but are not further discussed hereafter. For more details in those experiments the reader is referred to the literature [3]–[6]

Generation of extreme plasma conditions by irradiation of nano-wire arrays:

Ultrahigh-energy density (UHED) matter, characterized by energy densities $>1 \times 10^8 \text{ J cm}^{-3}$ and pressures $> 1 \text{ Gbar}$, is encountered in the center of stars and inertial confinement fusion capsules driven by the world's largest lasers. UHED conditions can be obtained with compact, ultrahigh contrast, femtosecond lasers focused to relativistic intensities onto targets composed of aligned nanowire arrays. We measured the key physical process in determining the energy density deposited in high-aspect-ratio nanowire array plasmas: the energy penetration. By monitoring the x-ray emission from buried Co tracer segments in Ni nanowire arrays irradiated at an intensity of $4 \times 10^{19} \text{ W cm}^{-2}$, we demonstrated energy penetration depths of several micrometers, leading to UHED plasmas of micrometer size. Relativistic three-dimensional particle-in-cell simulations, validated by these measurements, predict that irradiation of nanostructures at in-

tensities $>1 \times 10^{22} \text{ W cm}^{-2}$ will lead to a virtually unexplored extreme UHED plasma regime characterized by energy densities in excess of $8 \times 10^{10} \text{ J cm}^{-3}$, equivalent to a pressure of 0.35 Tbar. [3]

Generation of hard x-ray flashes:

The efficient conversion of optical laser light into bright ultrafast x-ray pulses in laser created plasmas is of high interest for dense plasma physics studies, material science and other fields. We have demonstrated more than one order of magnitude increase in picosecond x-ray conversion efficiency (CE) by tailoring near solid density plasmas to achieve a large radiative to hydrodynamic energy loss rate ratio, leading into a radiation loss dominated plasma regime. A record 20% CE into $h\nu >1 \text{ keV}$ photons was measured in arrays of large aspect ratio Au nanowires heated to keV temperatures with ultrahigh contrast femtosecond laser pulses of relativistic intensity. [4]

Electron/Ion acceleration:

By using a ultra-intense high contrast laser pulse with intensities of $1 \times 10^{21} \text{ W cm}^{-2}$ we were able to see significant improvement in both the flux and energy of the relativistic accelerated electrons of a near-solid density aligned CD_2 nanowire arrays in comparison to those from solid CD_2 foils irradiated with the same laser pulses. Because the laser is able to penetrate deep into the aligned nanowires, we were able to increase the volume of the interaction. The laser interaction with the nanowire was modeled and showed that electrons are pulled up the nanowire to the top and to a lower density plasma and there the electrons are accelerated up to the dephasing length, where they outrun the laser pulse. This results in an electron temperature that is much higher and larger flux than the flat foils. This interaction compared to the flat foil also produces many more 1 MeV photons. Utilising this method of irradiating nanowires we have also measured the acceleration of deuterons and hydrogen ions up to 15 MeV from CD_2 nanowire arrays measuring both the energy and the angular distribution.

Neutron generation:

While nuclear fusion in laser created plasmas is regularly created in spherical plasma compressions driven by multi-kilojoule pulses from the world's largest lasers, it is also of interest

to generate neutron source for applications that include neutron imaging and material diagnostics. We have demonstrated a dense micro-scale deuterium-deuterium (D-D) fusion environment created by irradiating arrays of deuterated nanostructures with joule-level pulses from a compact ultrafast laser. The irradiation of ordered deuterated polyethylene nanowires arrays with femtosecond pulses of relativistic intensity created ultra-high energy density plasmas in which deuterons are accelerated up to MeV energies, efficiently driving D-D fusion reactions and ultrafast neutron bursts. We measured up to 2×10^6 fusion neutrons per joule, an increase of about 500 times with respect to flat solid targets, a record yield for joule-level lasers. [6]

This dissertation describes the development of the petawatt-class laser system used at CSU for which the author was a major contributor. The description of the laser and its performance is followed by two application experiments: a plasma based soft x-ray laser and the use of a soft x-ray laser to perform single shot, large field of view nano-holography.

1.1 Petawatt-class laser systems

The desire to have more intense lasers for applications has been around since the beginning of lasers in 1960. In 1962 McClung and Hellwarth [7] were able to make lasers many orders of magnitude more intense than the first Ruby laser developed by Theodore Maiman in 1960 [8]. They accomplished this by changing the loss in a laser cavity from high to low usually using a Pockel cell and a set of polarizers, a technique known as Q-switching. By crossing the polarizers the loss in the cavity is very high, allowing a large population inversion to build up while the laser is pumped by avoiding lasing. When the gain reaches its peak the Pockel cell is triggered to rapidly rotate the polarization, lowering the cavity loss below the threshold for lasing. Q-switch lasers are commonly used in many fields of research and industry and create a millijoule level nanosecond pulse out of an oscillator. One year later in 1963 the method of mode-locking pushed durations to the picosecond range [9]. Mode-locking oscillators were able to produce femtosecond pulses but with nanojoules of energy per pulse [10]. Mode-locking and Q-switching were combined to create intense laser pulses of short duration. Shorter and more

intense pulses did not see much progress till the mid-1980s when the technique of chirp pulse amplification (CPA) was combined with mode-locking. In this technique pulses are spectrally chirped and stretched in time, amplified and finally recompressed. The first use of CPA was in radar systems. The idea of CPA was first applied to laser amplification by Strickland and Mourou in 1985 [11] a realization for which they were awarded the Nobel Prize in Physics in 2018. The method implementation with lasers starts with a short pulse that is stretched in time, amplified and is finally compressed to a short duration using diffraction gratings. By stretching the pulses out for amplification and only compressing the pulses right before transmission high peak powers within the amplifier are avoided. In its first demonstration Strickland and Mourou used a mode-locked Nd:YAG oscillator to produce a short 150 ps pulse. This pulse was then stretched in an optical fiber to 300 ps. The pulse was subsequently amplified with a Nd:YAG regenerative amplifier. The pulse was then compressed using a Treacy grating pair to 2 ps pulse duration [12]. The compressor was able to compensate the dispersion. The scheme was later improved by substituting the fiber stretcher with a grating stretcher that better matches the compressor and stretcher, consisting of a Treacy compressor with a telescope that inverts the sign of the dispersion, and innovation introduced by Martinez (Martinez 1987, [13]). Another advantage of the use of CPA is to be able to reach the saturation fluence. Laser materials like Nd:Glass have high saturation fluences of the order of joules per cm^2 . By stretching the pulse in time, it is possible to reach the saturation fluences without non-linear effects spoiling the wavefront. CPA opened the path to multi-Terawatt lasers, and eventually to Petawatt lasers. A diagram illustrating the concept of CPA systems is shown in Figure 1.1. Using this technique in 1989, the first 100 TW class laser was developed in France [14], [15] and in the UK [16], [17]. Each system utilized a Nd based mode-locked system relying on a self-phase modulation to create the needed bandwidth to support the short picosecond pulses at under 0.5 ps at 1054 nm [18]. The amplifiers were based on Nd:glass.

There are more than 50 petawatt lasers in operation in the world [20] with most of them falling into two main categories. Lasers with high amounts of energy with hundreds of Joules



figures/chap1fig11.png

Figure 1.1: Illustration of a classic CPA laser system. Inspired by [19].

or even kilojoules of energy with longer pulse duration on the order of several hundreds of femtoseconds [21], [22], and lasers that have less energy on the order of tens of Joules but much shorter pulse durations of the order of a few tens of femtoseconds [23]–[26]. The first category is limited in repetition rate to a few shots per day. This limitation mainly comes from the limitation in the repetition rate of the pump lasers, this is related to their cool down time. The category of high energy, long pulse petawatt lasers dates back to 1992, when scientists at Lawrence Livermore National Laboratory (LLNL) [27] developed the first petawatt laser, the NOVA petawatt. It was able to deliver 1.5 PW with 660 J in a 440 fs. The NOVA petawatt laser was focused to intensities of $7 \times 10^{20} \text{ W cm}^2$. This laser was followed by the Vulcan Laser, a high power Nd:glass laser, and was the first to implement the optical parametric chirped pulse amplification (OPCPA) front end [28], [29]. The OPCPA is able to amplify ultrashort and broadband pulses with little pre-pulse and thus have higher contrast. When this is injected into the Nd:glass amplifier chain it is able to produce short and high contrast pulses and is used as a front end for many petawatt lasers today. Some of the other petawatt laser around the world

are the Gekko XII facility in Japan. It used an OPCPA front end with Nd:glass large aperture amplifiers, and a double pass compressor to with an output of 420 J in a 470 fs pulse. The Gekko XII is focused to intensities of 2.5×10^{19} W/cm² with contrast levels of 1.5×10^8 [30]. Titan is a laser at LLNL that delivers up to 300 J in a sub-picosecond pulse and offers a 50 J high contrast green option [31].



Figure 1.2: Evolution of the laser spectra through the system: after stretcher (dotted line); after first power amplifier (dashed line); after compressor (solid line); and the final spectral phase (dash-dotted line).

In the second category of petawatt lasers based on lower energy but much shorter pulses the most common gain media used is Ti:sapphire. Ti:Sapphire has a broad spectral bandwidth (>235 nm FWHM) [32] and thus is able to support a shorter pulse. As an example the spectral output of the amplified pulses from the Ti:Sapphire oscillator at CSU is shown in Figure 1.2. This Ti:Sapphire oscillator output has a bandwidth of about 30nm FWHM and can support ~ 30 fs transform limited laser pulses. Shorter pulses dramatically help in making higher intensities. Some of the properties of Ti:Sapphire that also contribute to it being a favorable gain material are high damage threshold, good thermal conductivity, and a saturation fluence of 1-2 J/cm² [33]. The passive Kerr lens was implemented in the mode-locked Ti:Sapphire oscillator for even better

outcomes [10]. Soon after this improvement the first terawatt Ti:Sapphire laser was demonstrated by Sullivan et al. [34]. With an output of 3.8 terawatts, this laser ran at 10Hz and had pulses with outputs of 60 fs and 0.23 J. With Ti:Sapphire having a upper level lifetime of $\sim 3 \mu s$ the gain medium cannot be efficiently pumped with flashlamps and needs a fast pumping method. Since Ti:Sapphire has a high absorption in the 500 nm region of the spectrum a doubled $\sim 1.0 \mu m$ laser is usually used as the pump.

Notable examples of petawatt-class higher repetition rate lasers are the BELLA laser at Lawrence Berkeley National Laboratory with an output of 1.3 PW and a repetition rate of 1 Hz [35], the 1 PW HAPLS laser designed at LLNL to operate at repetition rates up to 10 Hz and recently operated at 3.3 Hz [36], and the 3.3 Hz CSU laser reported in this dissertation. All three of these petawatt-class and many other high power ultrashort pulse lasers operating with pulse widths in the vicinity of 30 fs are made employing Ti:Sapphire as the gain medium [23]–[26], [37]–[43]. Ti:Sapphire can presently reach peak powers of up to 5.4 PW [25] and a lasers with outputs of 10 PWs are about to be commissioned[44], [45]. OPCPA petawatt lasers also have short pulse durations, wider bandwidth, high temporal contrast, small thermal effects and tunable wavelengths [23], [24], [26] but for the most part do not have as high an energy because of the lower efficiency achieved to date in converting the pump light into OPCPA output.

The petawatt laser system at CSU that the author of this dissertation co-developed is a CPA Ti:Sapphire laser centered at 800 nm with a bandwidth shown in Figure 1.2. It is able to produce laser pulses with 25.5 J after compression with pulse duration of 30 fs making it 0.85 PWs. It is also able to run at a repetition rate of 3.3 Hz making it the highest repetition rate petawatt laser in the world. There are plans for the production of petawatt laser systems to improve on CSU's repetition rate with ELI (European Light Infrastructure) with a repetition rate of 10 Hz and an output of one petawatt [46]. Since the CSU CPA petawatt laser is a key aspect of the work performed by the author as part of this dissertation a more detailed look at all the aspects of this kind of laser as it relates to the petawatt lasers will be in what follows. A closer look at the CSU petawatt laser will be in Chapter 2.

1.2 Petawatt-class Chirped Pulse Amplification Lasers

A CPA system typically achieves high energy pulses with multiple stages of amplification [11]. The CSU petawatt-class lasers makes use of a conventional front-end. Ultrashort pulses are generated by a Kerr-lens mode-locked Ti:Sapphire oscillator. These pulses are subsequently stretched by a Martinez stretcher [13] and are then amplified by five Ti:Sapphire stages of amplification. They are finally recompressed by a grating compressor [12]. For some specific applications (for example x-ray laser generation) a fraction of the beam is split before compression and directed to the target chamber creating a longer pre-pulse. Figure 1.3 shows a schematic diagram illustrating the different stages of the CPA laser system. After the stretcher and before the first amplifier an acousto optic programmable diffuse filter (AOPDF) is placed to modify the amplitudes of specific wavelengths for the purpose discussed below. Between each stage of amplification there is an imaging vacuum telescope (VT) used to expand the beam to match the stage's pump laser mode. Spatial filters (SF) are placed at the focus of these telescopes to remove any high frequency structure from the beam's intensity profile. Isolation between the first three amplifiers is provided by a Pockels cell (PC) and polarizing beam splitters (PBS). The PBS pairs are crossed to avoid transmission unless the PC rotates the polarization of the laser pulse. This is necessary to reduce amplified spontaneous emission (ASE) feedback between the high gain amplifiers which can reduce energy extraction. If a sufficiently small temporal window is created with the Pockels cell the isolation combination along with the spatial filters can also reject any stray back reflections that may arise in the system. This can reduce the possibility of high intensity focuses that can damage components. A deformable mirror (DM) is also installed after the five stages of amplification to correct any wavefront aberrations. Each part of the system is discussed in more detail below.

1.2.1 Laser Oscillator

The seed pulse for the petawatt laser is generated by a mode-locked oscillator. The basic cavity configuration is shown in Figure 1.4. The oscillator pump source is a commercially fre-

figures/chap1fig13.png

Figure 1.3: Schematic diagram of Ti:Sapphire CPA laser system developed at CSU.

quency doubled Nd:YVO₄ diode-pumped continuous wave (cw) laser. This cw green laser light is focused into the Ti:Sapphire crystal, collinear with the mode of the laser cavity itself. The only other cavity components are an end mirror (M), curved mirrors (CM), an output coupler (OC) and together with a prism pair (P1, P2) to compensate for dispersion of the Ti:Sapphire crystal [47]. Mode-locking in this laser is achieved through the action of the Kerr lens induced in the laser crystal itself. When the laser is operating in a pulsed mode, the focused intensity inside the Ti:Sapphire crystal exceeds 10^{11} W/cm². This is sufficient to induce a strong non-linear lens which significantly focuses the pulse. When this occurs in a laser cavity which is adjusted for optimum efficiency without this lens, the self-focusing will simply contribute to loss within the laser cavity. However, modest displacement of one mirror away from the optimum cw position by only 0.5-1 mm can result in a decrease in loss in the laser cavity when Kerr lensing is present. To understand this, suppose some modes incidentally are phase locked and interfere constructively forming a pulse that has higher intensity than the modes with random phases. These pulses are focused and thereby collimated in the cavity, surviving and seeing gain with low loss. All other modes that are not affected are thus not collimated and are rejected by suffering high losses. This allows the in phase high intensity modes to "win out" and reach relatively high energy. Very quickly only modes oscillating in phase creating the mode-locked pulses survive. Thus, the Kerr lensing couples the spatial and temporal modes of the oscillator, resulting in two distinct spatial and temporal modes of operation (cw and pulsed) [48]. The laser can be aligned to be stable in either mode.

The oscillator in the CSU petawatt-class laser is based on a kit by KM Labs that produces 30 fs pulses at 87MHz with $\sim 750\text{mW}$. The output spectrum is shown in Figure 1.2. A 4 W Nd:YVO4 diode 532nm laser (Coherent-Verdi) is used to pump the Ti:Sapphire crystal. To compensate for the self-phase modulation and group velocity dispersion from the $\sim 4.5\text{ mm}$ 15% doped Ti:Sapphire crystal, a pair of prisms (P1, P2) is used to sustain the short pulses as shown in Figure 1.4. Two concave mirrors (CM) are used to focus the 800nm beam in the Ti:Sapphire rod to create the intensities needed to operate the oscillator in the Kerr-lens mode locked operation. Mirror (M) is used to keep the beam in the cavity and a 17% output coupler (OC) is used to eject the beam to the rest of the system.



Figure 1.4: Schematic Diagram of the Ti:Sapphire Oscillator. The Nd:YVO4 diode 532nm laser (Coherent-Verdi) is the pump the mirrors M and Prism pair P1,P2 and the curved dichroic mirrors CM and output coupler OC.

1.2.2 Stretcher and Compressor

Once out of the oscillator the pulses are injected into the stretcher to stretch the pulse in time through a positive dispersion delay stage. After the stretcher the pulse is modified by the acousto optic programmable diffuse filter and then is amplified. Once amplified the pulse is then compressed back to a short pulse in a negative dispersion delay stage. Both the stretcher and the compressor work to complement each other by exactly undoing what the other does. The



figures/chap1fig15a.png

(a)



figures/chap1fig15b.png

(b)

Figure 1.5: (a) Schematic layout of a grating-based stretcher leading to a positive dispersion. (b) Schematic layout of a grating-based compressor with negative dispersion. [49]

stretcher is designed to stretch a pulse from 30 fs to ~ 500 ps, reducing the intensity by a factor of ~ 16600 . The compressor reverses this effect and it also is aligned to compensate as much as possible for any dispersion picked up by the pulse traveling through the Ti:Sapphire crystal, windows and air.

The main component in both stretching and compressing is the grating. In the stretcher and compressor it is necessary to avoid nonlinear distortion to the spatial and temporal profile of the beam. A chirped pulse can be obtained by propagating a pulse through optical material such as a fiber. In the fiber, self-phase modulation (SPM) can broaden the bandwidth of the pulse; however the distortion due to high-order phase terms introduced by fiber are hard to compensate and makes this design difficult to use for femtosecond pulse amplifiers. To obtain an even greater stretch factors, a grating or prism pair arrangement can be used which separates the spectrum of a short pulse in such a way that different colors follow different paths through the optical system.

Martinez et al. [13] realized that by placing a telescope between a grating pair, and an injection and sendback mirror as shown in Figure 1.5a, the dispersion is controlled by the effective distance between the second grating and the image of the first grating [13]. If the distance given by L is smaller than f ($L < f$) the stage will add positive group delay dispersion to the pulse given by:

$$\frac{\delta^2 \phi}{\delta \omega^2} = -\frac{2(L-f)N^2 \lambda^2}{\pi c^2 \cos^2 \theta} \quad (1.1)$$

Where L is the distance of the grating from the lens, c is the speed of light, λ is the center wavelength, N is the groove density (1/mm) and θ is the diffracted angle. In this arrangement the dispersion is exactly the opposite dispersion of a grating compressor. If $L > f$ the stage will put negative dispersion on the pulse making the telescope not needed and thus making a grating compressor shown in Figure 1.5b. This forms the basis for a perfectly matched stretcher/compressor pair. The change in pulse duration after the stretcher is given geometrically by:

$$\Delta \tau = \frac{L_g \left(\frac{\lambda}{d}\right) \Delta \lambda}{c d \left(1 - \left(\frac{\lambda}{d} - \sin \gamma\right)^2\right)} \quad (1.2)$$

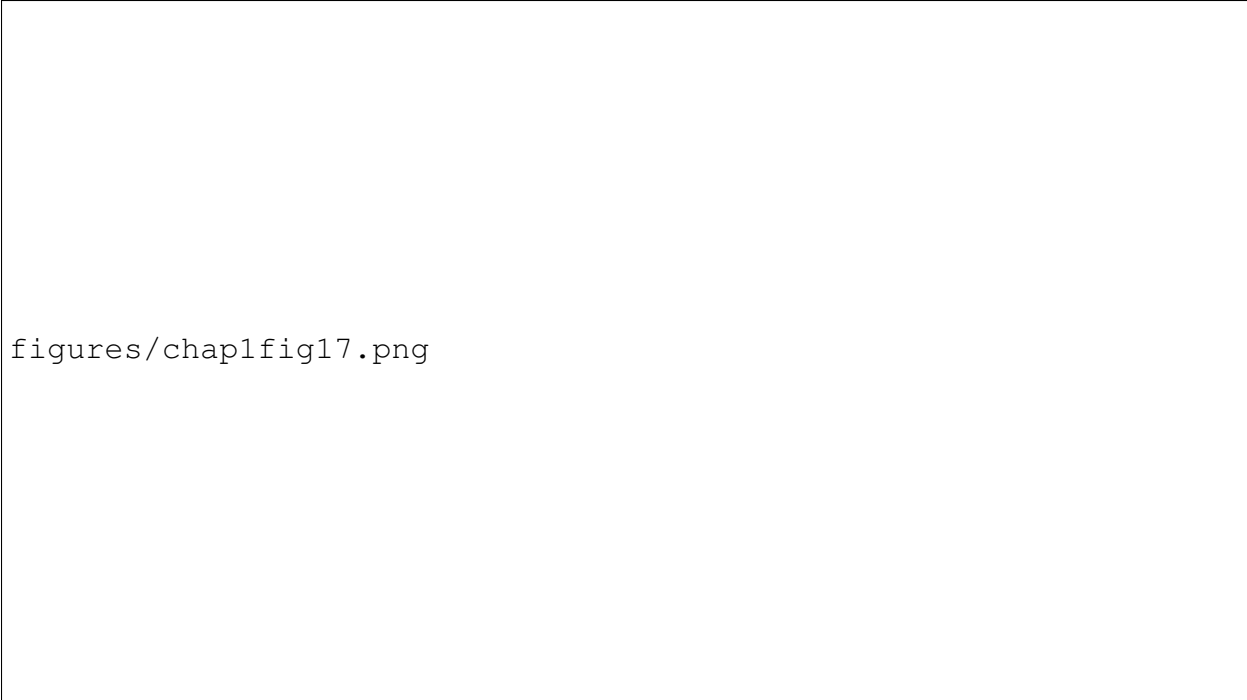
Where L_g is the grating separation (in the case of a stretcher it is equal to $2(L-f)$), c is the speed of light, λ is the center wavelength, $\Delta \lambda$ is the bandwidth of the laser pulse, d is the groove spacing and γ is the angle of incidence on the first grating with respect to normal. This stretcher configuration can be improved with the flat normal incident mirror placed at the focal plane. By using a curved mirror instead of lenses it is possible to avoid the chromatic aberrations of the lenses. With these changes the number of optics is reduced and there is only a need for one grating, which offers important advantages over the two grating designs. The grating can work near Littrow incident angle (given by $\sin \gamma_{Littrow} = \lambda/2d$), and maintain alignment while the separation and/or angle of the grating are adjusted. The single-grating design is also an advantage as there are no possibilities of anti-parallelism or angle mismatch between the gratings, which would distort the output pulse by introducing temporal and spatial chirps that cannot be eliminated in the pulse compressor. In Figure 1.6 shows the diagram of the computed

ray path for the folded telescope stretcher used at CSU. This setup uses a spherical focusing mirror with a radius of curvature of ~ 1200 mm corresponding to a focal length of ~ 600 mm and a diameter of 8 inches. The grating are gold coated and have 1740 l/mm with a Littrow angle of 44.1 degrees. The input angle to the grating is 55 degrees from normal. The separation of the center of the spherical mirror and the center of the grating is ~ 400 mm. With these parameters the calculated stretch is ~ 500 ps. The experimental setup is shown in the photograph below in Figure 1.7.



Figure 1.6: Simulation of the folded telescope stretcher.

As stated earlier the grating compressor, as shown in Figure 1.5b, allows us to recombine a chirped pulse that has been stretched. In 1969, Treacy showed that a pair of identical parallel gratings exhibits negative group delay dispersion [12]. The equation 1.2 is what is needed to calculate the compression with L_g simply being the distance between the gratings. We need to consider not only the contributions of the stretcher and the compressor, but also the materials of the amplifier. When a pulse passes through a material, the longer wavelengths travel faster than



figures/chap1fig17.png

Figure 1.7: Photograph of stretcher at CSU with simulation lines overlaid to guide the eye.

the shorter wavelengths, thus introducing a positive chirp on the pulse. This chirp must also be compensated for by the pulse compressor. The phase introduced by a material is given by:

$$\phi_{mat}(\omega) = L_{mat}n(\omega)\frac{\omega}{c} \quad (1.3)$$

Where L_{mat} is the material length, ω is the light frequency, c is the speed of light and $n(\omega)$ is the index of refraction. Expressions for $n(\lambda)$ can be obtained by empirical formulas (such as Sellmeier equations [50]) for common optical materials are tabulated in the literature. However, since analytic derivatives are much more accurate than performing a numerical polynomial fit to a curve, it is most accurate to work with the exact expressions for the phase, and not with terms in the Taylor expansion. The compressor used at CSU consists of four gold gratings with two being 210 mm \times 420mm \times 50 mm for the first and last grating and two 210 mm \times 460 mm \times 50 mm for the second and third grating. All the gratings have 1740 l/mm and were made by LLNL. The separation between the two gratings is \sim 725 mm. The compressor also has a 45 degree turning mirror 300.0 mm \times 210.0 mm \times 50.0 mm and two roof mirrors each 325.0

mm \times 300 mm \times 50.0 mm to translate the beam between the two grating levels. This is shown in Figure 2.3 and in Figure 2.4. Each optics in a custom mount designed and build in house. The grading mounts were also made in house and were made to have tip and tilt and rotation independently for each grating insuring the ability to align the two gratings that were stacked over each other to be both in the same parallel plane and also the grating lines aligned.

1.2.3 Amplification

The amplification chain uses a high gain pre-amplifier stage, placed just after the pulse stretcher, which is designed to increase the energy of the nJ pulses from the laser oscillator to the 1-10 mJ level [51]–[59]. The majority of the gain of the amplifier system ($\sim 10^7$ times) occurs in this stage. The pre-amplifier is then followed by four power amplifiers designed to efficiently extract the stored energy in the amplifier and to increase the output pulse power above the 30 joule level. At each stage there are different challenges that are needed to overcome in order to make an effective petawatt laser. For the first stage amplifier or pre-amplifier the main challenge is gain narrowing. Since the atomic susceptibility $X''(\omega)$ appears in the exponent in calculating the power gain, the exponential gain falls off much more rapidly with detuning than the atomic lineshape itself. Successive passes through the amplifier tends to narrow the amplified spectrum, as can be seen from:

$$G(\omega) = e^{\left[\frac{4.34\omega_a L}{c} X''(\omega)\right]} \quad (1.4)$$

where $X''(\omega)$ is the atomic susceptibility, L is the length of the laser path in the crystal, c is the speed of light and ω_a is the center frequency [60]. This spectral narrowing associated with the amplification process is referred to as gain narrowing. This narrowing restricts the compression transform limit of the pulse at the end of amplification. Since the gain profile of Ti:Sapphire falls more steeply at wavelengths shorter than 800 nm than at wavelengths longer than 800 nm, and since gain saturation tends to redshift the spectrum (red wavelengths precede blue in the pulse), the optimum input spectrum is typically peaked shorter than 800 nm. One tool to over-



(a)



(b)

Figure 1.8: (a) Illustration of gain narrowing (Fourier transform FFT) (b) Illustration of gain preservation by "burning" hole in the spectrum.

come this narrowing is the use of an AOPDF. With this filter it is possible to modulate both the phase and the amplitude of the spectrum [61]. By measuring the phase and length of the pulse after the amplification it is possible to optimize the input to create a flat phase and to preserve the bandwidth. The bandwidth is preserved by reducing the amplitude of the wavelengths that have the strongest gain and letting the other wavelengths dominate. By letting the wavelengths in the tail of the gain profile have a head start the final result is a wider bandwidth. An illustration of this process is shown in Figure 1.8. When this hole is burnt into the spectrum there is a loss in the seed energy. To compensate for this energy loss the beam pass one more time through the amplifier or pump the amplifier harder to increase the gain. A balance between pumping hard and extra passes is needed. The balance is between burning the optical coating and extracting the energy.

Nonlinear contributions to the phase resulting from self-phase modulation in the amplifier medium [62] must also be minimized to avoid self-focusing and self-phase modulation. The non-

linear phase shift is properly considered in the time domain, as $\phi_{NL}(t) = (2\pi/\lambda)n_2 \int I(t, z)dz$. However, since the pulse is chirped, this nonlinear temporal phase maps into the spectral phase. The approximate value of the nonlinear phase contribution is given by:

$$\phi_{nonlinear}(t) = \int \frac{2\pi}{\lambda} n_2 I(t, l) dl \quad (1.5)$$

where n_2 is the nonlinear index ($\sim 2.5 \times 10^{-16} \text{ cm}^2 \text{ W}^{-1}$ for sapphire) and $I(t, l)$ is the intensity within the amplifier material. The peak value of this expression is also known as the "B integral" of the amplifier system. The value of the B integral (the nonlinear phase shift at peak intensity) at which the nonlinear phase is important for pulse compression can be estimated as follows. The nonlinear group delay is approximately $d\phi/d\omega = B/\Delta\omega$, where $\Delta\omega$ is the half-width of the amplified spectrum. A B integral of 1 rad over a spectral half-width of 20 nm would add an additional delay variation of 17 fs. While this may to some extent be compensated by readjustment of the compressor, the value of the nonlinear phase varies across the beam, so severe distortions may still occur. Thus, it is clearly advantageous where possible to maintain the value of the B integral at less than 1.

One other problem that arises from a high B integral is self-focusing due to a Kerr lens. As the beam propagates through a material areas of higher intensity will have a delayed phase and this will act as a lens in that area. As this area focuses more it becomes even more intense and can have a runaway effect to cause a total collapse of the beam or sections of it. This can create a very intense energy that can focus in the optical material causing damage and distorting the beam profile and wavefront. By keeping the B integral below 1 this effect is avoided.

1.2.4 Mitigation of parasitic lasing

As the gain region becomes larger like those found in the power amplifiers of a Ti:Sapphire system there is a larger concern for parasitic lasing. Parasitic lasing is when the ASE that is emitted randomly in all directions in a gain medium starts to lase inside the crystal usually using



Figure 1.9: (a) Illustration of Ti:Sapphire crystal surrounded with air and a graph of gain vs pump fluence[63] (b) Illustration of Ti:Sapphire crystal surrounded with Cargille Series M refractive index liquid and a graph of output vs pump energy[63]

the lateral faces of the crystal as mirrors. This lasing in the crystal extracts energy in unwanted ways. Parasitic lasing happens in crystals with high gain or crystals with long gain pathways. In Ti:Sapphire systems when the crystals are pumped in large areas there are long transvers paths that can cause parasitic lasing if no precautions are taken. To avoid parasitic lasing it is important to keep the reflection of radial rays in the periphery of the crystals to a minimum. This can be achieved by putting an index matched liquid or cladding in the periphery of the crystal to avoid having reflected ASE from going back to the pumped volume of the crystal where the gain is high. To insure there is no reflected light from where the cladding ends or the liquid stops, an absorbent dye in the cladding or liquid is placed to absorb the light. A key aspect of this technique of this is making sure the refractive index of the matching liquid or cladding is close to that of the gain medium. The high index of refraction of Ti:Sapphire, 1.76 at 800 nm, makes it difficult to find a liquid with a similar index. There is a company "Cargille" that produces high index fluids (Cargille Series M refractive index liquid $n = 1.76$ at laser wavelength) that can match the index. The Cargille Series M refractive index liquid has many restrictions as

it is not compatible with many common materials such as steel, aluminum and copper alloys. Based on the compatibility report of Cargille Laboratories [64], we chose aluminum after a hard black anodization. This liquid is also very harmful when coming in contact with skin or when breathing its fumes. While this liquid was investigated and tested and used by other petawatt lasers [65] we opted for the liquid methyl salicylate (also known as wintergreen oil) that has an index of refraction of 1.53 at 800 nm. While Methyl salicylate has a lower index it also has the advantage of having lower health risks. Our tests found it to be sufficient for our case. Methyl salicylate is flowed around the Ti:Sapphire crystals and is cooled to 15 C with a heat exchanger to help with cooling of the crystals. An illustration of a crystal and boundary interaction and parasitic lasing is shown in Figure 1.9 along with examples of measurements [63].

Other ways to help eliminate parasitic lasing is to extract the energy before the gain becomes too high for parasitic lasing to extract the energy. This is achieved by having the laser pulse go through the crystal to extract the energy while the pump light is still pumping the crystal [66]. By timing the multiple passes of the laser pulses with respect to the pump pulses it is possible to efficiently extract the energy. This method has the drawback of being more complicated.

1.3 Foreword

The following chapters discuss the specifics of the laser system that I help make and design at CSU. This laser has been used in many experiments and has become a laser facility in Laser-NetUS. The next chapter focuses on the advances I was able to make in the field of x-ray lasers that extended the operation of gain-saturated compact repetitive x-ray lasers down to $\lambda = 6.85$ nm in Ni-like Gd. I was also able to show lasing at 6.67 nm and 6.11 nm in Ni-like Tb and amplification at 6.41 nm and 5.85 nm in Ni-like Dy. The next chapter describes experiments with single shot nano holography with resolutions of 62 nm and with time resolutions of 5 ps of 200 nm silver nano wires.

Bibliography

- [1] C. Danson, D. Hillier, N. Hopps, and D. Neely, “Petawatt class lasers worldwide,” *High Power Laser Science and Engineering*, vol. 3, Jan. 2015. DOI: 10.1017/hpl.2014.52.
- [2] A. Rockwood, Y. Wang, S. Wang, M. Berrill, V. N. Shlyaptsev, and J. J. Rocca, “Compact gain-saturated x-ray lasers down to 6.85 nm and amplification down to 5.85 nm,” *Optica*, vol. 5, no. 3, pp. 257–262, Mar. 2018. DOI: 10.1364/OPTICA.5.000257. [Online]. Available: <http://www.osapublishing.org/optica/abstract.cfm?URI=optica-5-3-257>.
- [3] C. Bargsten, R. Hollinger, M. G. Capeluto, V. Kaymak, A. Pukhov, S. Wang, A. Rockwood, Y. Wang, D. Keiss, R. Tommasini, R. London, J. Park, M. Busquet, M. Klapisch, V. N. Shlyaptsev, and J. J. Rocca, “Energy penetration into arrays of aligned nanowires irradiated with relativistic intensities: Scaling to terabar pressures,” *Science Advances*, vol. 3, no. 1, 2017. DOI: 10.1126/sciadv.1601558. eprint: <http://advances.sciencemag.org/content/3/1/e1601558.full.pdf>. [Online]. Available: <http://advances.sciencemag.org/content/3/1/e1601558>.
- [4] R. Hollinger, C. Bargsten, V. Shlyaptsev, V. Kaymak, A. Pukhov, M. Capeluto, S. Wang, A. Rockwood, Y. Wang, A. Townsend, A. Prieto, P. Stockton, A. Curtis, and J. Rocca, “Efficient picosecond x-ray pulse generation from plasmas in the radiation dominated regime,” *Optica*, vol. 4, p. 1344, Nov. 2017. DOI: 10.1364/OPTICA.4.001344.
- [5] A. Moreau, R. Hollinger, C. Calvi, S. Wang, Y. Wang, M. G. Capeluto, A. Rockwood, A. Curtis, S. Kasdorf, V. N. Shlyaptsev, V. Kaymak, A. Pukhov, and J. J. Rocca, “Enhanced electron acceleration in aligned nanowire arrays irradiated at highly relativistic intensities,” *Plasma Physics and Controlled Fusion*, vol. 62, no. 1, p. 014013, Nov. 2019. DOI: 10.1088/1361-6587/ab4d0c. [Online]. Available: <https://doi.org/10.1088%2F1361-6587%2Fab4d0c>.
- [6] A. Curtis, C. Calvi, J. Tinsley, R. Hollinger, V. Kaymak, A. Pukhov, S. Wang, A. Rockwood, Y. Wang, V. Shlyaptsev, and J. Rocca, “Micro-scale fusion in dense relativistic nanowire

- array plasmas,” *Nature Communications*, vol. 9, Dec. 2018. DOI: 10.1038/s41467-018-03445-z.
- [7] F. J. McClung and R. W. Hellwarth, “Giant optical pulsations from ruby,” *Appl. Opt.*, vol. 1, no. S1, pp. 103–105, Jan. 1962. DOI: 10.1364/AO.1.S1.000103. [Online]. Available: <http://ao.osa.org/abstract.cfm?URI=ao-1-101-103>.
- [8] T. H. Maiman, “Stimulated Optical Radiation in Ruby,” vol. 187, no. 4736, pp. 493–494, Aug. 1960. DOI: 10.1038/187493a0.
- [9] L. E. Hargrove, R. L. Fork, and M. A. Pollack, “Locking of He-Ne Laser Modes Induced by Synchronous Intracavity Modulation,” *Applied Physics Letters*, vol. 5, pp. 4–5, Jul. 1964. DOI: 10.1063/1.1754025.
- [10] D. E. Spence, P. N. Kean, and W. Sibbett, “60-fsec pulse generation from a self-mode-locked ti:sapphire laser,” *Opt. Lett.*, vol. 16, no. 1, pp. 42–44, Jan. 1991. DOI: 10.1364/OL.16.000042. [Online]. Available: <http://ol.osa.org/abstract.cfm?URI=ol-16-1-42>.
- [11] D. Strickland and G. Mourou, “Compression of amplified chirped optical pulses,” *Optics Communications*, vol. 56, pp. 219–221, Dec. 1985. DOI: 10.1016/0030-4018(85)90120-8.
- [12] E. Treacy, “Optical pulse compression with diffraction gratings,” *IEEE Journal of Quantum Electronics*, vol. 5, pp. 454–458, Sep. 1969. DOI: 10.1109/JQE.1969.1076303.
- [13] O. Martinez, “3000 times grating compressor with positive group velocity dispersion: Application to fiber compensation in 1.3-1.6 μm region,” *IEEE Journal of Quantum Electronics*, vol. 23, no. 1, pp. 59–64, Jan. 1987, ISSN: 0018-9197. DOI: 10.1109/JQE.1987.1073201.
- [14] C. Rouyer, É. Mazataud, I. Allais, A. Pierre, S. Seznec, C. Sauteret, G. Mourou, and A. Migus, “Generation of 50-tw femtosecond pulses in a ti:sapphire/nd:glass chain,” *Opt. Lett.*, vol. 18, no. 3, pp. 214–216, Feb. 1993. DOI: 10.1364/OL.18.000214. [Online]. Available: <http://ol.osa.org/abstract.cfm?URI=ol-18-3-214>.

- [15] N. Blanchot, C. Rouyer, C. Sauteret, and A. Migus, “Amplification of sub-100-tw femtosecond pulses by shifted amplifying nd:glass amplifiers: Theory and experiments,” *Opt. Lett.*, vol. 20, no. 4, pp. 395–397, Feb. 1995. DOI: 10.1364/OL.20.000395. [Online]. Available: <http://ol.osa.org/abstract.cfm?URI=ol-20-4-395>.
- [16] C. Danson, L. Barzanti, Z. Chang, A. Damerell, C. Edwards, S. Hancock, M. Hutchinson, M. Key, S. Luan, R. Mahadeo, I. Mercer, P. Norreys, D. Pepler, D. Rodkiss, I. Ross, M. Smith, R. Smith, P. Taday, W. Toner, and A. Zhou, “High contrast multi-terawatt pulse generation using chirped pulse amplification on the vulcan laser facility,” *Optics Communications*, vol. 103, pp. 392–397, Dec. 1993. DOI: 10.1016/0030-4018(93)90163-Y.
- [17] P. K. Rambo, I. C. Smith, J. L. Porter, M. J. Hurst, C. S. Speas, R. G. Adams, A. J. Garcia, E. Dawson, B. D. Thurston, C. Wakefield, J. W. Kellogg, M. J. Slattery, H. C. Ives, R. S. Broyles, J. A. Caird, A. C. Erlandson, J. E. Murray, W. C. Behrendt, N. D. Neilsen, and J. M. Narduzzi, “Z-beamlet: A multikilojoule, terawatt-class laser system,” *Appl. Opt.*, vol. 44, no. 12, pp. 2421–2430, Apr. 2005. DOI: 10.1364/AO.44.002421. [Online]. Available: <http://ao.osa.org/abstract.cfm?URI=ao-44-12-2421>.
- [18] M. W. Phillips, J. R. M. Barr, D. W. Hughes, D. C. Hanna, Z. Chang, C. N. Danson, and C. B. Edwards, “Self-starting additive-pulse mode locking of a nd:lma laser,” *Opt. Lett.*, vol. 17, no. 20, pp. 1453–1455, Oct. 1992. DOI: 10.1364/OL.17.001453. [Online]. Available: <http://ol.osa.org/abstract.cfm?URI=ol-17-20-1453>.
- [19] V. Chvykov, “New generation of ultra-high peak and average power laser systems,” in Oct. 2018, ISBN: 978-1-78923-740-5. DOI: 10.5772/intechopen.70720.
- [20] C. Danson, D. Hillier, N. Hopps, and D. Neely, “Petawatt class lasers worldwide,” *High Power Laser Science and Engineering*, vol. 3, e3, 2015. DOI: 10.1017/hpl.2014.52.
- [21] E. W. Gaul, M. Martinez, J. Blakeney, A. Jochmann, M. Ringuette, D. Hammond, T. Borger, R. Escamilla, S. Douglas, W. Henderson, G. Dyer, A. Erlandson, R. Cross, J. Caird, C. Ebberts, and T. Ditmire, “Demonstration of a 1.1 petawatt laser based on a hybrid optical

- parametric chirped pulse amplification/mixed nd:glass amplifier,” *Appl. Opt.*, vol. 49, no. 9, pp. 1676–1681, Mar. 2010. DOI: 10.1364/AO.49.001676. [Online]. Available: <http://ao.osa.org/abstract.cfm?URI=ao-49-9-1676>.
- [22] Y. Kitagawa, H. Fujita, R. Kodama, H. Yoshida, S. Matsuo, T. Jitsuno, T. Kawasaki, H. Kitamura, T. Kanabe, S. Sakabe, K. Shigemori, N. Miyanaga, and Y. Izawa, “Prepulse-free petawatt laser for a fast ignitor,” *IEEE Journal of Quantum Electronics*, vol. 40, no. 3, pp. 281–293, Mar. 2004, ISSN: 0018-9197. DOI: 10.1109/JQE.2003.823043.
- [23] J. H. Sung, H. W. Lee, J. Y. Yoo, J. W. Yoon, C. W. Lee, J. M. Yang, Y. J. Son, Y. H. Jang, S. K. Lee, and C. H. Nam, “4.2 pw, 20 fs ti:sapphire laser at 0.1 hz,” *Opt. Lett.*, vol. 42, no. 11, pp. 2058–2061, Jun. 2017. DOI: 10.1364/OL.42.002058. [Online]. Available: <http://ol.osa.org/abstract.cfm?URI=ol-42-11-2058>.
- [24] Z. Wang, C. Liu, Z. Shen, Q. Zhang, H. Teng, and Z. Wei, “High-contrast 1.16 pw ti:sapphire laser system combined with a doubled chirped-pulse amplification scheme and a femtosecond optical-parametric amplifier,” *Opt. Lett.*, vol. 36, no. 16, pp. 3194–3196, Aug. 2011. DOI: 10.1364/OL.36.003194. [Online]. Available: <http://ol.osa.org/abstract.cfm?URI=ol-36-16-3194>.
- [25] Z. Gan, L. Yu, S. Li, C. Wang, X. Liang, Y. Liu, W. Li, Z. Guo, Z. Fan, X. Yuan, L. Xu, Z. Liu, Y. Xu, J. Lu, H. Lu, D. Yin, Y. Leng, R. Li, and Z. Xu, “200 j high efficiency ti:sapphire chirped pulse amplifier pumped by temporal dual-pulse,” *Opt. Express*, vol. 25, no. 5, pp. 5169–5178, Mar. 2017. DOI: 10.1364/OE.25.005169. [Online]. Available: <http://www.opticsexpress.org/abstract.cfm?URI=oe-25-5-5169>.
- [26] X. Zeng, K. Zhou, Y. Zuo, Q. Zhu, J. Su, X. Wang, X. Wang, X. Huang, X. Jiang, D. Jiang, Y. Guo, N. Xie, S. Zhou, Z. Wu, J. Mu, H. Peng, and F. Jing, “Multi-petawatt laser facility fully based on optical parametric chirped-pulse amplification,” *Opt. Lett.*, vol. 42, no. 10, pp. 2014–2017, May 2017. DOI: 10.1364/OL.42.002014. [Online]. Available: <http://ol.osa.org/abstract.cfm?URI=ol-42-10-2014>.

- [27] M. D. Perry, D. Pennington, B. C. Stuart, G. Tietbohl, J. A. Britten, C. Brown, S. Herman, B. Golick, M. Kartz, J. Miller, H. T. Powell, M. Vergino, and V. Yanovsky, “Petawatt laser pulses,” *Opt. Lett.*, vol. 24, no. 3, pp. 160–162, Feb. 1999. DOI: 10.1364/OL.24.000160. [Online]. Available: <http://ol.osa.org/abstract.cfm?URI=ol-24-3-160>.
- [28] I. N. Ross, J. L. Collier, P. Matousek, C. N. Danson, D. Neely, R. M. Allott, D. A. Pepler, C. Hernandez-Gomez, and K. Osvay, “Generation of terawatt pulses by use of optical parametric chirped pulse amplification,” *Appl. Opt.*, vol. 39, no. 15, pp. 2422–2427, May 2000. DOI: 10.1364/AO.39.002422. [Online]. Available: <http://ao.osa.org/abstract.cfm?URI=ao-39-15-2422>.
- [29] J. Collier, C. Hernandez-Gomez, I. N. Ross, P. Matousek, C. N. Danson, and J. Walczak, “Evaluation of an ultrabroadband high-gain amplification technique for chirped pulse amplification facilities,” *Appl. Opt.*, vol. 38, no. 36, pp. 7486–7493, Dec. 1999. DOI: 10.1364/AO.38.007486. [Online]. Available: <http://ao.osa.org/abstract.cfm?URI=ao-38-36-7486>.
- [30] M. Mori, Y. Kitagawa, R. Kodama, H. Habara, M. Iwata, S. Tsuji, K. Suzuki, K. Sawai, K. Tanaka, Y. Kato, and K. Mima, “Ultra intense glass laser system and laser-plasma interactions,” *Nuclear Instruments and Methods in Physics Research A*, vol. 410, pp. 367–372, Feb. 1998. DOI: 10.1016/S0168-9002(98)00151-X.
- [31] B. C. Stuart, J. D. Bonlie, J. A. Britten, J. A. Caird, R. Cross, C. A. Ebberts, M. J. Eckart, A. C. Erlandson, W. A. Molander, A. Ng, P. K. Patel, and D. F. Price, “The titan laser at llnl,” in *Conference on Lasers and Electro-Optics/Quantum Electronics and Laser Science Conference and Photonic Applications Systems Technologies*, Optical Society of America, 2006, JTuG3. [Online]. Available: <http://www.osapublishing.org/abstract.cfm?URI=CLEO-2006-JTuG3>.
- [32] P. F. Moulton, “Spectroscopic and laser characteristics of ti:al₂o₃,” *J. Opt. Soc. Am. B*, vol. 3, no. 1, pp. 125–133, Jan. 1986. DOI: 10.1364/JOSAB.3.000125. [Online]. Available: <http://josab.osa.org/abstract.cfm?URI=josab-3-1-125>.

- [33] S. Backus, C. G. Durfee, M. M. Murnane, and H. C. Kapteyn, “High power ultrafast lasers,” *Review of Scientific Instruments*, vol. 69, no. 3, pp. 1207–1223, 1998. DOI: 10.1063/1.1148795. eprint: <https://doi.org/10.1063/1.1148795>. [Online]. Available: <https://doi.org/10.1063/1.1148795>.
- [34] A. Sullivan, H. Hamster, H. C. Kapteyn, S. Gordon, W. White, H. Nathel, R. J. Blair, and R. W. Falcone, “Multiterawatt, 100-fs laser,” *Opt. Lett.*, vol. 16, no. 18, pp. 1406–1408, Sep. 1991. DOI: 10.1364/OL.16.001406. [Online]. Available: <http://ol.osa.org/abstract.cfm?URI=ol-16-18-1406>.
- [35] W. P. Leemans, J. Daniels, A. Deshmukh, A. Gonsalves, A. Magana, H. Mao, D. Mittelberger, K. Nakamura, J. Riley, D. Syversrud, C. Toth, and N. Ybarrolaza, “Bella laser and operations*,” 2013.
- [36] *Llnl meets key milestone for delivery of world’s highest average power petawatt laser system*, Feb. 2017. [Online]. Available: <https://www.llnl.gov/news/llnl-meets-key-milestone-delivery-worldE28099s-highest-average-power-petawatt-laser-system>.
- [37] K. Nakamura, H. Mao, A. J. Gonsalves, H. Vincenti, D. E. Mittelberger, J. Daniels, A. Magana, C. Toth, and W. P. Leemans, “Diagnostics, control and performance parameters for the bella high repetition rate petawatt class laser,” *IEEE Journal of Quantum Electronics*, vol. 53, no. 4, pp. 1–21, Aug. 2017, ISSN: 0018-9197. DOI: 10.1109/JQE.2017.2708601.
- [38] L. Xu, L. Yu, X. Liang, Y. Chu, Z. Hu, L. Ma, Y. Xu, C. Wang, X. Lu, H. Lu, Y. Yue, Y. Zhao, F. Fan, H. Tu, Y. Leng, R. Li, and Z. Xu, “High-energy noncollinear optical parametric chirped pulse amplification in lbo at 800 nm,” *Opt. Lett.*, vol. 38, no. 22, pp. 4837–4840, Nov. 2013. DOI: 10.1364/OL.38.004837. [Online]. Available: <http://ol.osa.org/abstract.cfm?URI=ol-38-22-4837>.
- [39] M. M. Aleonard, M. Altarelli, P. Antici, A. Apolonskiy, P. Audebert, A. Bartnik, C. Barty, A. Bernstein, J. Biegert, P. Bfffdfffdni, N. Booth, D. Bote, S. V. Bulanov, R. Butkus, L. Cardoso, J. Chambaret, D. Charambilidis, G. Cheriaux, R. Clarke, and M. Zepf, *WHITEBOOK*

- ELI - Extreme Light Infrastructure; Science and Technology with Ultra-Intense Lasers*. Jan. 2011. DOI: 10.13140/2.1.1227.0889.
- [40] C. Hernandez-Gomez, S. P. Blake, O. Chekhlov, R. J. Clarke, A. M. Dunne, M. Galimberti, S. Hancock, R. Heathcote, P. Holligan, A. Lyachev, P. Matousek, I. O. Musgrave, D. Neely, P. A. Norreys, I. Ross, Y. Tang, T. B. Winstone, B. E. Wyborn, and J. Collier, “The vulcan 10 PW project,” *Journal of Physics: Conference Series*, vol. 244, no. 3, p. 032 006, Aug. 2010. DOI: 10.1088/1742-6596/244/3/032006.
- [41] E. Khazanov, “Nonlinear optics: East-west reunion,” *Institute of Applied Physics*, 2011.
- [42] J. P. Zou, *Invited talk at hplse 2014*, 2014.
- [43] S. Backus, C. G. Durfee, M. M. Murnane, and H. C. Kapteyn, “High power ultrafast lasers,” *Review of Scientific Instruments*, vol. 69, no. 3, pp. 1207–1223, 1998. DOI: 10.1063/1.1148795. eprint: <https://doi.org/10.1063/1.1148795>. [Online]. Available: <https://doi.org/10.1063/1.1148795>.
- [44] B. Le Garrec, D. Papadopoulos, C. Le Blanc, J.-P. Zou, A. Frfffdfffdneaux, L. Martin, N. Lebas, A. Beluze, F. Mathieu, P. Audebert, G. Cheriaux, P. Georges, and F. Druon, “Design update and recent results of the apollon 10 pw facility,” Jan. 2017, SF1K.3. DOI: 10.1364/CLEO_SI.2017.SF1K.3.
- [45] F. Lureau, S. Laux, O. Casagrande, O. Chalus, P. Duvochelle, S. Herriot, G. Matras, C. Radier, L. Boudjemaa, C. Simon-Boisson, R. Dabu, I. Dancus, and D. Ursescu, “Design and initial results of 10 pw laser for eli-np,” in *2015 European Conference on Lasers and Electro-Optics - European Quantum Electronics Conference*, Optical Society of America, 2015, CF_{P20}. [Online]. Available: http://www.osapublishing.org/abstract.cfm?URI=CLEO_Europe-2015-CF_P_20.
- [46] S. Karsch, Z. Major, J. Fülöp, I. Ahmad, T.-J. Wang, A. Henig, S. Kruber, R. Weingartner, M. Siebold, J. Hein, C. Wandt, S. Klingebiel, J. Osterhoff, R. Horlein, and F. Krausz, “The petawatt field synthesizer: A new approach to ultrahigh field generation,” in *Advanced Solid-*

- State Photonics*, Optical Society of America, 2008, WF1. DOI: 10.1364/ASSP.2008.WF1. [Online]. Available: <http://www.osapublishing.org/abstract.cfm?URI=ASSP-2008-WF1>.
- [47] R. L. Fork, O. E. Martinez, and J. P. Gordon, “Negative dispersion using pairs of prisms,” *Opt. Lett.*, vol. 9, no. 5, pp. 150–152, May 1984. DOI: 10.1364/OL.9.000150. [Online]. Available: <http://ol.osa.org/abstract.cfm?URI=ol-9-5-150>.
- [48] I. P. Christov, H. C. Kapteyn, M. M. Murnane, C.-P. Huang, and J. Zhou, “Space–time focusing of femtosecond pulses in a ti:sapphire laser,” *Opt. Lett.*, vol. 20, no. 3, pp. 309–311, Feb. 1995. DOI: 10.1364/OL.20.000309. [Online]. Available: <http://ol.osa.org/abstract.cfm?URI=ol-20-3-309>.
- [49] H.-K. Nienhuys. (2019). Cpastretcher.svg, [Online]. Available: https://commons.wikimedia.org/wiki/File:Cpa_stretcher.svg.
- [50] M. Bass and O. S. of America, *Handbook of Optics: Fundamentals, techniques, and design*, ser. Handbook of Optics v. 1. McGraw-Hill, 1994, ISBN: 9780070477407. [Online]. Available: <https://books.google.com/books?id=ggc6AQAAIAAJ>.
- [51] J. Zhou, C.-P. Huang, C. Shi, M. M. Murnane, and H. C. Kapteyn, “Generation of 21-fs millijoule-energy pulses by use of ti:sapphire,” *Opt. Lett.*, vol. 19, no. 2, pp. 126–128, Jan. 1994. DOI: 10.1364/OL.19.000126. [Online]. Available: <http://ol.osa.org/abstract.cfm?URI=ol-19-2-126>.
- [52] S. Backus, J. Peatross, C. P. Huang, M. M. Murnane, and H. C. Kapteyn, “Ti:sapphire amplifier producing millijoule-level, 21-fs pulses at 1 khz,” *Opt. Lett.*, vol. 20, no. 19, pp. 2000–2002, Oct. 1995. DOI: 10.1364/OL.20.002000. [Online]. Available: <http://ol.osa.org/abstract.cfm?URI=ol-20-19-2000>.
- [53] J. V. Rudd, G. Korn, S. Kane, J. Squier, G. Mourou, and P. Bado, “Chirped-pulse amplification of 55-fs pulses at a 1-khz repetition rate in a ti:al₂o₃ regenerative amplifier,” *Opt. Lett.*, vol. 18, no. 23, pp. 2044–2046, Dec. 1993. DOI: 10.1364/OL.18.002044. [Online]. Available: <http://ol.osa.org/abstract.cfm?URI=ol-18-23-2044>.

- [54] C. L. Blanc, G. Grillon, J. P. Chambaret, A. Migus, and A. Antonetti, “Compact and efficient multipass ti:sapphire system for femtosecond chirped-pulse amplification at the terawatt level,” *Opt. Lett.*, vol. 18, no. 2, pp. 140–142, Jan. 1993. DOI: 10.1364/OL.18.000140. [Online]. Available: <http://ol.osa.org/abstract.cfm?URI=ol-18-2-140>.
- [55] M. Lenzner, C. Spielmann, E. Wintner, F. Krausz, and A. J. Schmidt, “Sub-20-fs, kilohertz-repetition-rate ti:sapphire amplifier,” *Opt. Lett.*, vol. 20, no. 12, pp. 1397–1399, Jun. 1995. DOI: 10.1364/OL.20.001397. [Online]. Available: <http://ol.osa.org/abstract.cfm?URI=ol-20-12-1397>.
- [56] F. Salin, J. Squier, G. Mourou, and G. Vaillancourt, “Multikilohertz ti:al₂O₃ amplifier for high-power femtosecond pulses,” *Opt. Lett.*, vol. 16, no. 24, pp. 1964–1966, Dec. 1991. DOI: 10.1364/OL.16.001964. [Online]. Available: <http://ol.osa.org/abstract.cfm?URI=ol-16-24-1964>.
- [57] J. Squier, S. Coe, K. Clay, G. A. Mourou, and D. Harter, “An alexandrite pumped nd:glass regenerative amplifier for chirped pulse amplification,” *Optics Communications*, vol. 92, pp. 73–78, Aug. 1992. DOI: 10.1016/0030-4018(92)90221-C.
- [58] G. Vaillancourt, T. B. Norris, J. S. Coe, P. Bado, and G. A. Mourou, “Operation of a 1-khz pulse-pumped ti:sapphire regenerative amplifier,” *Opt. Lett.*, vol. 15, no. 6, pp. 317–319, Mar. 1990. DOI: 10.1364/OL.15.000317. [Online]. Available: <http://ol.osa.org/abstract.cfm?URI=ol-15-6-317>.
- [59] K. Wynne, G. D. Reid, and R. M. Hochstrasser, “Regenerative amplification of 30-fs pulses in ti:sapphire at 5 khz,” *Opt. Lett.*, vol. 19, no. 12, pp. 895–897, Jun. 1994. DOI: 10.1364/OL.19.000895. [Online]. Available: <http://ol.osa.org/abstract.cfm?URI=ol-19-12-895>.
- [60] A. E. Siegman, *Lasers*. 1990.
- [61] F. Verluise, V. Laude, Z. Cheng, C. Spielmann, and P. Tournois, “Amplitude and phase control of ultrashort pulses by use of an acousto-optic programmable dispersive filter:pulse

- compression and shaping,” *Opt. Lett.*, vol. 25, no. 8, pp. 575–577, Apr. 2000. DOI: 10.1364/OL.25.000575. [Online]. Available: <http://ol.osa.org/abstract.cfm?URI=ol-25-8-575>.
- [62] M. D. Perry, T. Ditmire, and B. C. Stuart, “Self-phase modulation in chirped-pulse amplification,” *Opt. Lett.*, vol. 19, no. 24, pp. 2149–2151, Dec. 1994. DOI: 10.1364/OL.19.002149. [Online]. Available: <http://ol.osa.org/abstract.cfm?URI=ol-19-24-2149>.
- [63] X. Liang, Y. Leng, C. Wang, C. Li, L. Lin, B. Zhao, Y. Jiang, X. Lu, M. Hu, C. Zhang, H. Lu, D. Yin, Y. Jiang, X. Lu, H. Wei, J. Zhu, R. Li, and Z. Xu, “Parasitic lasing suppression in high gain femtosecond petawatt ti:sapphire amplifier,” *Opt. Express*, vol. 15, no. 23, pp. 15 335–15 341, Nov. 2007. DOI: 10.1364/OE.15.015335. [Online]. Available: <http://www.opticsexpress.org/abstract.cfm?URI=oe-15-23-15335>.
- [64] [Http://www.cargille.com](http://www.cargille.com).
- [65] Y. Chu, X. Liang, L. Yu, Y. Xu, L. Xu, L. Ma, X. Lu, Y. Liu, Y. Leng, R. Li, and Z. Xu, “High-contrast 2.0 petawatt ti:sapphire laser system,” *Opt. Express*, vol. 21, no. 24, pp. 29 231–29 239, Dec. 2013. DOI: 10.1364/OE.21.029231. [Online]. Available: <http://www.opticsexpress.org/abstract.cfm?URI=oe-21-24-29231>.
- [66] Y. Chu, Z. Gan, X. Liang, L. Yu, X. Lu, C. Wang, X. Wang, L. Xu, H. Lu, D. Yin, Y. Leng, R. Li, and Z. Xu, “High-energy large-aperture ti:sapphire amplifier for 5 pw laser pulses,” *Opt. Lett.*, vol. 40, no. 21, pp. 5011–5014, Nov. 2015. DOI: 10.1364/OL.40.005011. [Online]. Available: <http://ol.osa.org/abstract.cfm?URI=ol-40-21-5011>.

Chapter 2

0.85 PW Laser operation at 3.3 Hz and high-contrast ultrahigh-intensity $\lambda = 400$ nm second-harmonic beamline¹

2.1 Overview

This chapter discusses the generation of 0.85 PW, 30 fs laser pulses at a repetition rate of 3.3 Hz with a record average power of 85 W from a Ti:Sapphire laser. The system is pumped by high-energy Nd:glass slab amplifiers frequency doubled in LiB₃O₅ (LBO). Ultrahigh-contrast $\lambda = 400$ nm femtosecond pulses are generated in KH₂PO₄ (KDP) with >40% efficiency. An intensity of 6.5×10^{21} W/cm² is obtained by frequency doubling 80% of the available Ti:Sapphire energy and focusing the doubled light with an $f/2$ parabola. This laser will enable highly relativistic plasma experiments to be conducted at high repetition rate.

2.2 Development of the high peak power laser and its characteristics

There is great interest in ultrahigh-intensity laser pulses for relativistic ultrahigh-energy density science, ultrashort-wavelength coherent, incoherent radiation sources and particle acceleration. The advent of chirped-pulse amplification (CPA) [1] enabled dramatic growth in the peak power of the most powerful lasers [2], [3]. Several petawatt (PW) lasers have been demonstrated or are under development in laboratories worldwide [4]–[11]. New laser systems aimed to generate peak powers of 10 PW also are under development [12]–[16]. The first laser to achieve

¹Y. Wang et al. "0.85 PW Laser operation at 3.3 Hz and high-contrast ultrahigh-intensity $\lambda = 400$ nm second-harmonic beamline" Optics Letters Vol. 42, Issue 19, pp. 3828-3831 (2017) © 2017 Optical Society of America

the PW power level did so by compressing kJ pulses from an Nd:glass laser to ps pulse duration [4]. Other lasers achieved this peak power level with less energetic pulses of hundreds of J and hundreds of fs pulse duration from Nd:glass amplifiers [5], [6]. These lasers typically fire at a repetition rate of several shots per hour. A second class of PW-class lasers produces much less energetic pulses of shorter pulse duration, typically 30 fs or less [7]–[10]. To date, most PW lasers have been developed with Titanium:Sapphire (Ti:Sa) as the gain medium, which offers broad bandwidth and fs pulse duration [7]–[17]. Alternatively, the technique of optical parametric CPA applied to PW laser offers the advantages of a wider bandwidth, high temporal contrast, small thermal effects and tunable wavelength [7], [8], [10] but with typically lower efficiency. High-power Ti:Sa lasers were demonstrated at the >100 TW peak power level at 10 Hz repetition rate [3]. However, the repetition rate of such lasers decreases greatly as they are scaled to PW, mostly due to heat removal limitations in the pump lasers. The highest peak power achieved to date is a 5.4 PW Ti:Sa laser [9]. The highest repetition rate reported for PW class lasers is 1 Hz [11] and significantly less in most other cases [5], [6], [8]. A diode-pumped Nd:glass-pumped Ti:Sa laser is under development to generate PW pulses at 10 Hz [18]. Presently in the commissioning phase, this laser has so far been demonstrated to generate 16 J pulses at 3.3 Hz repetition rate that, once compressed, should produce >0.4 PW peak power pulses with an average power >40 W [18]. A Ti:Sa field synthesizer also is under development with the goal of reaching a PW level output at a repetition rate of 10 Hz [19]. While diode pumping of PW lasers has clear advantages for scaling to high repetition rates and increased efficiency, flash lamps still remain greatly more affordable. Here we report the demonstration of a flash-lamp-pumped Ti:Sa laser, which generates 0.85 PW pulses of 30 fs duration at 3.3 Hz repetition rate with a record average power of 85 W after compression. This is the highest average power reported to date for a PW class laser. The laser setup is schematically illustrated in Figure 2.1. It consists of a conventional Ti:Sa front end that delivers $\lambda = 800$ nm pulses into a chain of three high-power Ti:Sa amplification stages pumped by Nd:YAG slab amplifiers designed to operate at repetition rate up to 5 Hz. An 87 MHz Kerr lens mode-locked oscillator (KMLabs) produces 45 nm bandwidth pulses

that are stretched to 550 ps FWHM using a grating stretcher [20]. A Pockels cell selects pulses at a frequency of 10 Hz to match the repetition rate of the first two stages of Ti:Sa amplification. These low-energy multipass amplifiers generate 3 mJ and 250 mJ pulses when pumped by a commercially available 600 mJ, 10 Hz, frequency-doubled Q-switched Nd:YAG laser (Quanta Ray Pro-270).



Figure 2.1: Diagram of 3.3 Hz, 0.85 PW CPA Ti:Sa laser system. Top: Ti:Sa laser, frequency-doubling setup and target chamber. Bottom: Pump laser based on Nd:glass slab amplifiers designed to operate at a 5 Hz repetition rate. VT, vacuum tube; SA, serrated aperture; SF, spatial filter; AT, anamorphic telescope; WP, wave plate.

The output of this laser front end is further amplified in three multipass Ti:Sa amplifiers pumped by the frequency-doubled output of eight compact flash-lamp-pumped high-energy slab Nd:glass amplifiers, developed at CSU [21]. The front end of the slab laser system consists of a Q-switched 1053 nm Nd:YLF oscillator that produces 10 mJ pulses of ~ 15 ns FWHM duration. The pulses from this oscillator are relay imaged onto a serrated aperture to generate a flat-top beam profile and then spatially filtered to produce a beam with a super-Gaussian intensity

profile. This beam profile is relay imaged throughout the rest of the system. The pulses are first amplified to 100 mJ in a flash-lamp-pumped preamplifier consisting of two 7 mm diameter Nd:YLF rods. The beam size is subsequently enlarged and is amplified to 3 J passing through a combination of two 9 mm and two 15 mm Nd:YLF rods, all flash-lamp pumped. The amplified beam is subsequently split into two arms by a 50% beam splitter. Each beam arm is further amplified by an additional 15 mm Nd:YLF amplifier to reach an energy of 3 J. Both circular beams are subsequently stretched onto 8 mm \times 120 mm ovals using cylindrical anamorphic imaging telescopes to conform to the 10 mm \times 140 mm cross section of the slab amplifiers. The oval beam of each of the two arms is amplified in two passes through the 400 mm length of a Nd:glass slab preamplifier. This preamplifier and the final eight slab amplifiers are similar to those we previously used to pump a 7.5 J, 170 TW, Ti:Sa laser [21]. The narrow slab geometry with zig-zag beam path has long been recognized as a way to eliminate first-order thermal and stress-induced focusing, reduce stress-induced birefringence and increase heat removal to avoid stress induce fracture. This significantly reduces the limitations in the repetition rate inherent to the more commonly used rod geometry [22], [23]. Slab amplifiers have been previously used to amplify nanosecond pulses up to 25 J energy [24], [25]. Our Nd:glass slab pump laser amplifiers are pumped by four Xe flash lamps, which are driven with 300 μ s duration current pulses that deposit \sim 700 J of electrical energy per lamp per shot. The cooling is provided by turbulent water flow.

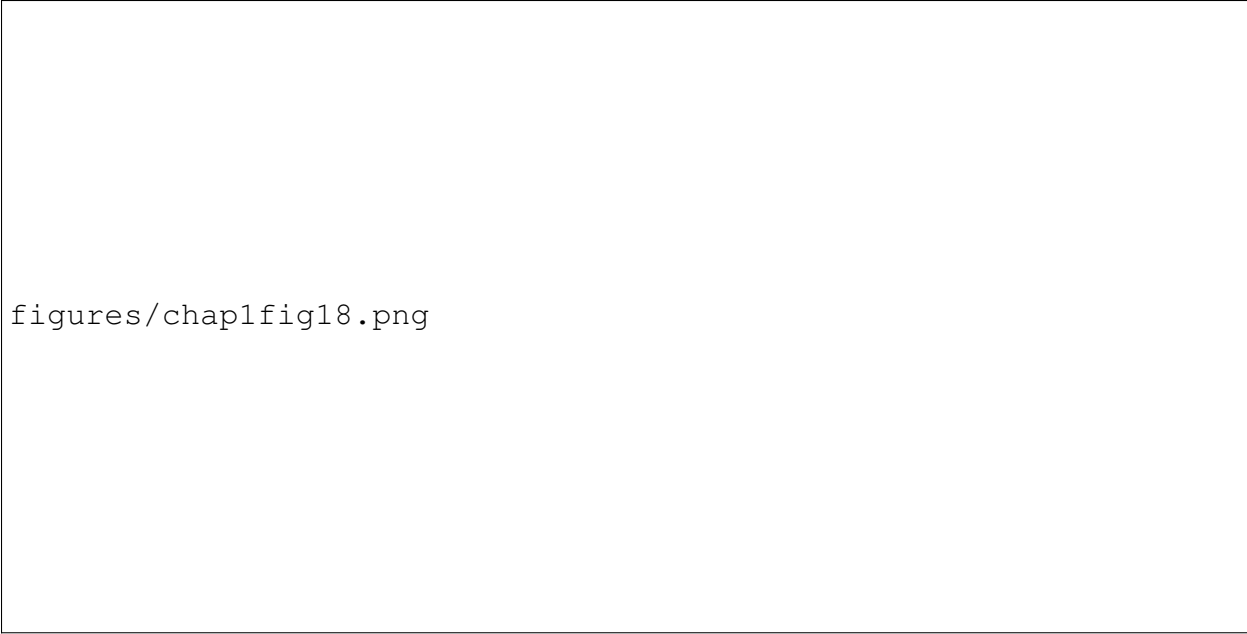
Each of the slab preamplifiers is operated to generate 16 J pulses that are divided evenly by three beam splitters (25%, 33%, 50%) to become the input of four identical Nd:glass slab power amplifiers. Amplification of input pulses with 4 J energy in each slab generates pulses with \sim 18 J energy and 15 ns duration at 1053 nm. The rms pulse energy fluctuation for 1053 nm slab pump laser is \sim 1%. The amplified beams are reshaped into 22 mm diameter beams that are imaged into 27 mm diameter LBO crystals (CrystalLaser) to generate 11 J pulses at 527 nm. The doubling efficiency is \sim 63%. A $\lambda/2$ wave plate is placed on each arm before the LBO crystal

to ensure S-polarization output. The eight slab amplifiers arms produce a total 527 nm pump energy of ~ 88 J, with a uniform nearly flat-top beam profile.

A 6 J pulse is separated and relay imaged onto the first of three high-power Ti:Sa amplification stages that use a 30 mm diameter, 28 mm thick crystal. Three passes of the 800 nm, 250 mJ seed pulses through this Ti:Sa amplifier produce pulse energies up to 3 J at 3.3 Hz repetition rate. From the remaining laser pump energy, 38 J pulses are relay imaged onto a fourth amplification stage, consisting of a 60 mm diameter, 30 mm thick Ti:Sa crystal in which the beam diameter is 45 mm. After two passes, the energy is 13.5 J. The remaining 44 J of laser pump energy are relay imaged onto a fifth stage amplifier, consisting of a 90 mm diameter, 30 mm thick, Ti:Sa crystal (GT Crystal Systems). The output energy can reach >37.6 J after three-pass amplification with a beam size of 55 mm. The crystals of the last two amplification stages are surrounded by flowing methyl salicylate for cooling and suppression of parasitic lasing. Because all the pump beams and the seed beam have flattop spatial profiles, the output beam is close to a homogeneous flattop (Figure 2.2).



Figure 2.2: Spatial single-shot beam profile after the final Ti:Sa booster amplifier operating at full power.

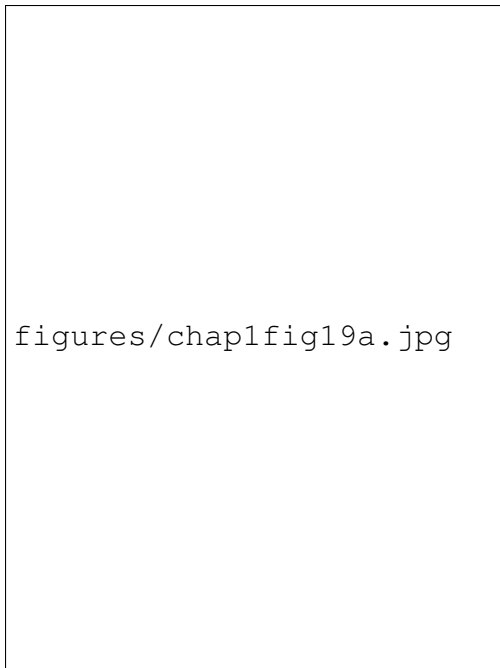


figures/chap1fig18.png

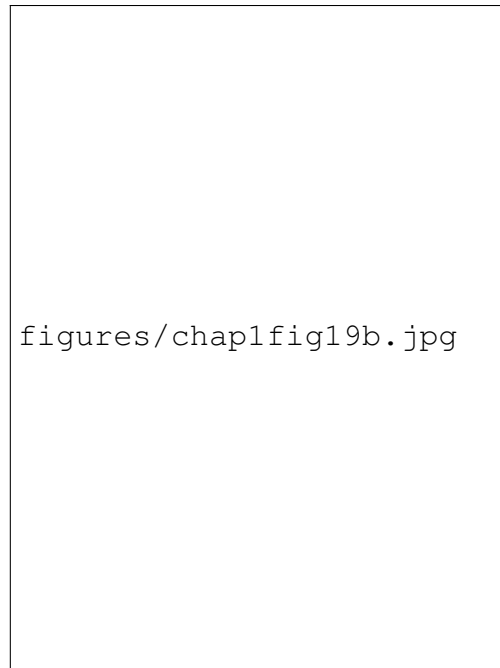
Figure 2.3: Simulation of the grating compressor at CSU.

The evolution of the laser spectrum along the amplifier chain is shown in Figure 1.2. An acousto-optic programmable dispersive filter (FASTLITE) is inserted between the stretcher and the first multipass amplifier to compensate for gain narrowing and to control redshift to broaden the bandwidth. The spectral bandwidth after the compressor is 50 nm FWHM. The B integral of the system is estimated to be 1.4.

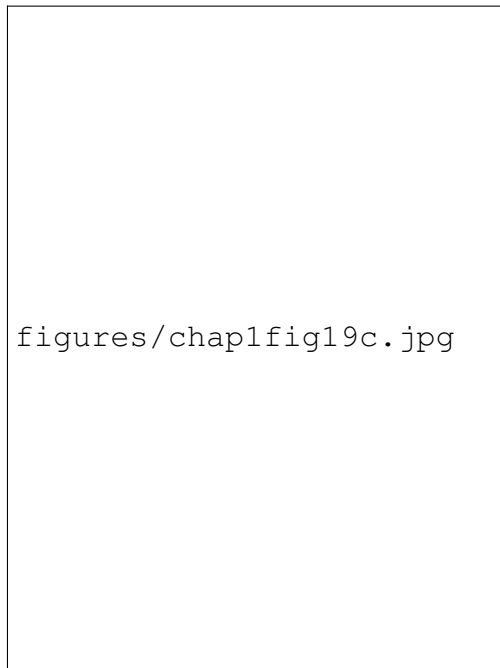
The output pulses are compressed in a vacuum gratings compressor composed of four 1740 l/mm gold-coated holographic gratings (Lawrence Livermore National Laboratory) [26]. A diagram of the compressor is shown in Figure 2.3. The first and fourth gratings are 42 cm \times 21 cm in size, and the second and third gratings are 46 cm \times 21 cm in size. The Gratings and roof mirrors are shown in Figure 2.4. The beam diameter is enlarged to 185 mm before entering the compressor using a reflective telescope. The total transmission efficiency of the compressor is 70%, resulting in compressed pulses of up to 26.3 J energy. The temporal intensity profile is reconstructed by a single-shot real-time spectral phase measurement device [27]. The measured compressed pulse duration is 30 fs (Figure 2.5), giving a peak power of \sim 0.88 PW for the highest energy shots produced. Figure 2.6 shows the shot-to-shot pulse energy variation measured before



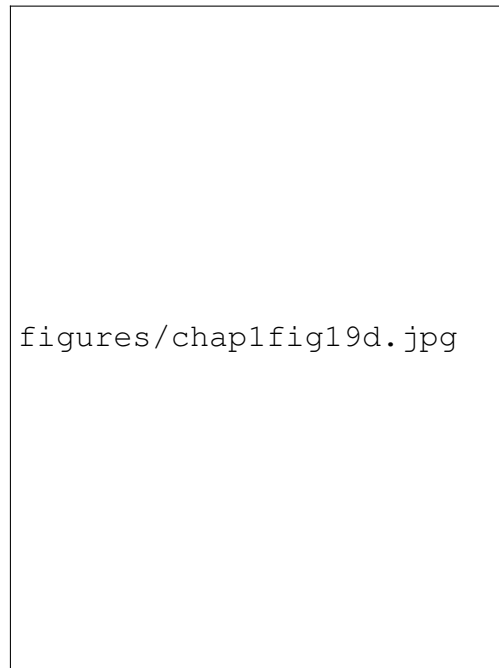
(a)



(b)



(c)



(d)

Figure 2.4: Photograph of gratings (a),(b) used at CSU, also the roof mirror (c) and turning mirror(d).

compressor for a series of consecutive shots at 3.3 Hz. The average pulse energy is 36.3 J, corresponding to an average power of 120 W before compression. The shot-to-shot energy variation is $\sim 1.7\%$ rms. The average pulse output energy after the compressor is 25.4 J, corresponding to

an average peak power of 0.85 PW and an average power of 85 W. This is the highest average power reported to date from a PW class laser. Operation of the pump laser at its full design goal of 5 Hz could potentially generate an average power of 127 W after compression.



Figure 2.5: Autocorrelation trace of the compressed pulses obtained from a single-shot real-time spectral phase measurement.

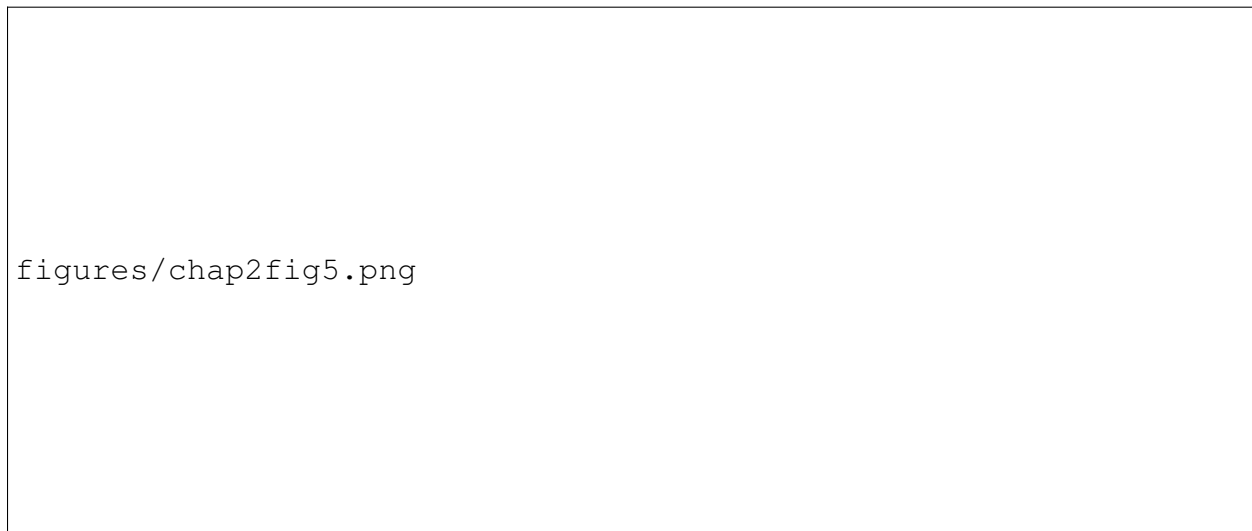


Figure 2.6: Shot-to-shot pulse energy variation of Ti:Sa laser pulse before compression at 3.3 Hz repetition rate.



Figure 2.7: Doubling efficiency as a function of input pulse energy. Inset: Spot focus with $f/2$ parabolic mirror at $\lambda = 400$ nm.

To enable experiments requiring ultrahigh contrast [28], the 30 fs, $\lambda=800$ nm laser output pulses were frequency doubled in a 0.8 mm thick antireflection coated KDP crystal. The beam diameter at the crystal is 185 mm. The $\lambda=400$ nm second harmonic light is separated from the 800 nm fundamental beam using a sequence of five dichroic mirrors with 99.9% reflectivity at $\lambda=400$ nm and a transmittance of $>99.5\%$ at the fundamental wavelength. A first set of frequency-doubling experiments was conducted using up to 80% of the output pulse energy available from the Ti:Sa laser. Figure 2.7 shows the measured doubling efficiency as a function of the energy impinging on the doubling crystal.

A conversion efficiency $>40\%$ is readily obtained for input intensities of 2×10^3 GW/cm², resulting in $\lambda = 400$ nm pulses of >8 J. Because the contrast of the $\lambda=800$ nm pulses was measured to be $\sim 5 \times 10^6$, the second-harmonic pulses are inferred to have a contrast $>1 \times 10^{12}$. Beam focusing is accomplished with an $f/2$ off-axis parabolic mirror (OAP) ($f=370$ mm). A deformable mirror placed after the last amplifier with Shack Hartmann sensor feedback was used to minimize

the spot focus diameter to $\sim 1.2 \mu\text{m}$ FWHM (Figure 2.7 inset), corresponding to an intensity of $\sim 6.5 \times 10^{21} \text{ W/cm}^2$. The use of an $f/1$ OAP will allow us to reach intensities $> 2 \times 10^{22} \text{ W/cm}^2$. An even higher intensity will be obtained using the full energy of the pulses generated by the PW class Ti:Sa laser.

2.3 Conclusions

In conclusion, we have demonstrated a Ti:Sa CPA laser that generates 0.85 PW pulses of 30 fs duration at 3.3 Hz repetition rate. This laser is enabled by a frequency-doubled high-energy flash-lamp-pumped Nd:glass zig-zag slab pump laser designed to operate at repetition rates up to 5 Hz with good beam quality. Pulses containing 80% of the maximum available energy were frequency doubled to generate ultrahigh-contrast $\lambda=400 \text{ nm}$ fs pulses, which were focused to obtain an intensity of $6.5 \times 10^{21} \text{ W/cm}^2$. Intensities $> 2 \times 10^{22} \text{ W/cm}^2$ will be obtainable using $f/1$ focusing optics. This PW-class laser will enable relativistic plasma experiments at high repetition rate and will extend high repetition rate soft x-ray lasers to shorter wavelengths.

Bibliography

- [1] D. Strickland and G. Mourou, "Compression of amplified chirped optical pulses," *Optics Communications*, vol. 56, pp. 219–221, Dec. 1985. DOI: 10.1016/0030-4018(85)90120-8.
- [2] C. P. J. Barty, T. Guo, C. Le Blanc, F. Raksi, C. Rose-Petruck, J. Squier, K. R. Wilson, V. V. Yakovlev, and K. Yamakawa, "Generation of 18-fs, multiterawatt pulses by regenerative pulse shaping and chirped-pulse amplification," *Optics Letters*, vol. 21, pp. 668–670, May 1996. DOI: 10.1364/OL.21.000668.
- [3] K. Yamakawa, M. Aoyama, S. Matsuoka, T. Kase, Y. Akahane, and H. Takuma, "100-tw sub-20-fs ti:sapphire laser system operating at a 10-hz repetition rate," *Opt. Lett.*, vol. 23, no. 18, pp. 1468–1470, Sep. 1998. DOI: 10.1364/OL.23.001468. [Online]. Available: <http://ol.osa.org/abstract.cfm?URI=ol-23-18-1468>.
- [4] M. D. Perry, D. Pennington, B. C. Stuart, G. Tietbohl, J. A. Britten, C. Brown, S. Herman, B. Golick, M. Kartz, J. Miller, H. T. Powell, M. Vergino, and V. Yanovsky, "Petawatt laser pulses," *Opt. Lett.*, vol. 24, no. 3, pp. 160–162, Feb. 1999. DOI: 10.1364/OL.24.000160. [Online]. Available: <http://ol.osa.org/abstract.cfm?URI=ol-24-3-160>.
- [5] E. W. Gaul, M. Martinez, J. Blakeney, A. Jochmann, M. Ringuette, D. Hammond, T. Borger, R. Escamilla, S. Douglas, W. Henderson, G. Dyer, A. Erlandson, R. Cross, J. Caird, C. Ebbers, and T. Ditmire, "Demonstration of a 1.1 petawatt laser based on a hybrid optical parametric chirped pulse amplification/mixed nd:glass amplifier," *Appl. Opt.*, vol. 49, no. 9, pp. 1676–1681, Mar. 2010. DOI: 10.1364/AO.49.001676. [Online]. Available: <http://ao.osa.org/abstract.cfm?URI=ao-49-9-1676>.
- [6] Y. Kitagawa, H. Fujita, R. Kodama, H. Yoshida, S. Matsuo, T. Jitsuno, T. Kawasaki, H. Kitamura, T. Kanabe, S. Sakabe, K. Shigemori, N. Miyanaga, and Y. Izawa, "Prepulse-free petawatt laser for a fast ignitor," *IEEE Journal of Quantum Electronics*, vol. 40, no. 3, pp. 281–293, Mar. 2004, ISSN: 0018-9197. DOI: 10.1109/JQE.2003.823043.

- [7] J. H. Sung, H. W. Lee, J. Y. Yoo, J. W. Yoon, C. W. Lee, J. M. Yang, Y. J. Son, Y. H. Jang, S. K. Lee, and C. H. Nam, “4.2 pw, 20 fs ti:sapphire laser at 0.1 hz,” *Opt. Lett.*, vol. 42, no. 11, pp. 2058–2061, Jun. 2017. DOI: 10.1364/OL.42.002058. [Online]. Available: <http://ol.osa.org/abstract.cfm?URI=ol-42-11-2058>.
- [8] Z. Wang, C. Liu, Z. Shen, Q. Zhang, H. Teng, and Z. Wei, “High-contrast 1.16 pw ti:sapphire laser system combined with a doubled chirped-pulse amplification scheme and a femtosecond optical-parametric amplifier,” *Opt. Lett.*, vol. 36, no. 16, pp. 3194–3196, Aug. 2011. DOI: 10.1364/OL.36.003194. [Online]. Available: <http://ol.osa.org/abstract.cfm?URI=ol-36-16-3194>.
- [9] Z. Gan, L. Yu, S. Li, C. Wang, X. Liang, Y. Liu, W. Li, Z. Guo, Z. Fan, X. Yuan, L. Xu, Z. Liu, Y. Xu, J. Lu, H. Lu, D. Yin, Y. Leng, R. Li, and Z. Xu, “200 j high efficiency ti:sapphire chirped pulse amplifier pumped by temporal dual-pulse,” *Opt. Express*, vol. 25, no. 5, pp. 5169–5178, Mar. 2017. DOI: 10.1364/OE.25.005169. [Online]. Available: <http://www.opticsexpress.org/abstract.cfm?URI=oe-25-5-5169>.
- [10] X. Zeng, K. Zhou, Y. Zuo, Q. Zhu, J. Su, X. Wang, X. Wang, X. Huang, X. Jiang, D. Jiang, Y. Guo, N. Xie, S. Zhou, Z. Wu, J. Mu, H. Peng, and F. Jing, “Multi-petawatt laser facility fully based on optical parametric chirped-pulse amplification,” *Opt. Lett.*, vol. 42, no. 10, pp. 2014–2017, May 2017. DOI: 10.1364/OL.42.002014. [Online]. Available: <http://ol.osa.org/abstract.cfm?URI=ol-42-10-2014>.
- [11] K. Nakamura, H. Mao, A. J. Gonsalves, H. Vincenti, D. E. Mittelberger, J. Daniels, A. Magana, C. Toth, and W. P. Leemans, “Diagnostics, control and performance parameters for the bella high repetition rate petawatt class laser,” *IEEE Journal of Quantum Electronics*, vol. 53, no. 4, pp. 1–21, Aug. 2017, ISSN: 0018-9197. DOI: 10.1109/JQE.2017.2708601.
- [12] L. Xu, L. Yu, X. Liang, Y. Chu, Z. Hu, L. Ma, Y. Xu, C. Wang, X. Lu, H. Lu, Y. Yue, Y. Zhao, F. Fan, H. Tu, Y. Leng, R. Li, and Z. Xu, “High-energy noncollinear optical parametric chirped pulse amplification in lbo at 800 nm,” *Opt. Lett.*, vol. 38, no. 22, pp. 4837–4840,

- Nov. 2013. DOI: 10.1364/OL.38.004837. [Online]. Available: <http://ol.osa.org/abstract.cfm?URI=ol-38-22-4837>.
- [13] M. M. Aleonard, M. Altarelli, P. Antici, A. Apolonskiy, P. Audebert, A. Bartnik, C. Barty, A. Bernstein, J. Biegert, P. Bfffdfffdni, N. Booth, D. Bote, S. V. Bulanov, R. Butkus, L. Cardoso, J. Chambaret, D. Charambilidis, G. Cheriaux, R. Clarke, and M. Zepf, *WHITEBOOK ELI - Extreme Light Infrastructure; Science and Technology with Ultra-Intense Lasers*. Jan. 2011. DOI: 10.13140/2.1.1227.0889.
- [14] C. Hernandez-Gomez, S. P. Blake, O. Chekhlov, R. J. Clarke, A. M. Dunne, M. Galimberti, S. Hancock, R. Heathcote, P. Holligan, A. Lyachev, P. Matousek, I. O. Musgrave, D. Neely, P. A. Norreys, I. Ross, Y. Tang, T. B. Winstone, B. E. Wyborn, and J. Collier, “The vulcan 10 PW project,” *Journal of Physics: Conference Series*, vol. 244, no. 3, p. 032 006, Aug. 2010. DOI: 10.1088/1742-6596/244/3/032006.
- [15] E. Khazanov, “Nonlinear optics: East-west reunion,” *Institute of Applied Physics*, 2011.
- [16] J. P. Zou, *Invited talk at hplse 2014*, 2014.
- [17] S. Backus, C. G. Durfee, M. M. Murnane, and H. C. Kapteyn, “High power ultrafast lasers,” *Review of Scientific Instruments*, vol. 69, no. 3, pp. 1207–1223, 1998. DOI: 10.1063/1.1148795. eprint: <https://doi.org/10.1063/1.1148795>. [Online]. Available: <https://doi.org/10.1063/1.1148795>.
- [18] E. Sistrunk, T. Spinka, A. Bayramian, S. Betts, R. Bopp, S. Buck, K. Charron, J. Cupal, R. Deri, M. Drouin, A. Erlandson, E. S. Fulkerson, J. Horner, J. Horacek, J. Jarboe, K. Kasl, D. Kim, E. Koh, L. Koubikova, R. Lanning, W. Maranville, C. Marshall, D. Mason, J. Menapace, P. Miller, P. Mazurek, A. Naylor, J. Novak, D. Peceli, P. Rosso, K. Schaffers, D. Smith, J. Stanley, R. Steele, S. Telford, J. Thoma, D. VanBlarcom, J. Weiss, P. Wegner, B. Rus, and C. Haefner, “All diode-pumped, high-repetition-rate advanced petawatt laser system (hapls),” in *Conference on Lasers and Electro-Optics*, Optical Society of America,

- 2017, STh1L.2. DOI: 10.1364/CLEO_SI.2017.STh1L.2. [Online]. Available: http://www.osapublishing.org/abstract.cfm?URI=CLEO_SI-2017-STh1L.2.
- [19] S. Karsch, Z. Major, J. Fülöp, I. Ahmad, T.-J. Wang, A. Henig, S. Kruber, R. Weingartner, M. Siebold, J. Hein, C. Wandt, S. Klingebiel, J. Osterhoff, R. Horlein, and F. Krausz, “The petawatt field synthesizer: A new approach to ultrahigh field generation,” in *Advanced Solid-State Photonics*, Optical Society of America, 2008, WF1. DOI: 10.1364/ASSP.2008.WF1. [Online]. Available: <http://www.osapublishing.org/abstract.cfm?URI=ASSP-2008-WF1>.
- [20] O. E. Martinez, J. P. Gordon, and R. L. Fork, “Negative group-velocity dispersion using refraction,” *J. Opt. Soc. Am. A*, vol. 1, no. 10, pp. 1003–1006, Oct. 1984. DOI: 10.1364/JOSAA.1.001003. [Online]. Available: <http://josaa.osa.org/abstract.cfm?URI=josaa-1-10-1003>.
- [21] D. H. Martz, D. Alessi, B. M. Luther, Y. Wang, D. Kemp, M. Berrill, and J. J. Rocca, “High-energy 13.9 nm table-top soft-x-ray laser at 2.5 hz repetition rate excited by a slab-pumped ti:sapphire laser,” *Opt. Lett.*, vol. 35, no. 10, pp. 1632–1634, May 2010. DOI: 10.1364/OL.35.001632. [Online]. Available: <http://ol.osa.org/abstract.cfm?URI=ol-35-10-1632>.
- [22] William S Martin, Joseph P Chernoch, *Multiple internal reflection face-pumped laser*, Jan. 1972.
- [23] J. Eggleston, T. Kane, K. Kuhn, J. Unternahrer, and R. Byer, “The slab geometry laser - part i: Theory,” *IEEE Journal of Quantum Electronics*, vol. 20, no. 3, pp. 289–301, Mar. 1984, ISSN: 0018-9197. DOI: 10.1109/JQE.1984.1072386.
- [24] C. B. Dane, L. E. Zapata, W. A. Neuman, M. A. Norton, and L. A. Hackel, “Design and operation of a 150 w near diffraction-limited laser amplifier with sbs wavefront correction,” *IEEE Journal of Quantum Electronics*, vol. 31, no. 1, pp. 148–163, Jan. 1995, ISSN: 0018-9197. DOI: 10.1109/3.341719.
- [25] M. J. Shoup, J. H. Kelly, and D. L. Smith, “Design and testing of a large-aperture, high-gain, brewster’s angle zigzag nd:glass slab amplifier,” *Appl. Opt.*, vol. 36, no. 24, pp. 5827–5838,

- Aug. 1997. DOI: 10.1364/AO.36.005827. [Online]. Available: <http://ao.osa.org/abstract.cfm?URI=ao-36-24-5827>.
- [26] J. A. Britten, M. D. Perry, B. W. Shore, and R. D. Boyd, “Universal grating design for pulse stretching and compression in the 800–1100-nm range,” *Opt. Lett.*, vol. 21, no. 7, pp. 540–542, Apr. 1996. DOI: 10.1364/OL.21.000540. [Online]. Available: <http://ol.osa.org/abstract.cfm?URI=ol-21-7-540>.
- [27] T. Oksenhendler, S. Coudreau, N. Forget, V. Crozatier, S. Grabielle, R. Herzog, O. Gobert, and D. Kaplan, “Self-referenced spectral interferometry,” *Applied Physics B*, vol. 99, no. 1, pp. 7–12, Apr. 2010, ISSN: 1432-0649. DOI: 10.1007/s00340-010-3916-y. [Online]. Available: <https://doi.org/10.1007/s00340-010-3916-y>.
- [28] C. Bargsten, R. Hollinger, M. G. Capeluto, V. Kaymak, A. Pukhov, S. Wang, A. Rockwood, Y. Wang, D. Keiss, R. Tommasini, R. London, J. Park, M. Busquet, M. Klapisch, V. N. Shlyaptsev, and J. J. Rocca, “Energy penetration into arrays of aligned nanowires irradiated with relativistic intensities: Scaling to terabar pressures,” *Science Advances*, vol. 3, no. 1, 2017. DOI: 10.1126/sciadv.1601558. eprint: <http://advances.sciencemag.org/content/3/1/e1601558.full.pdf>. [Online]. Available: <http://advances.sciencemag.org/content/3/1/e1601558>.

Chapter 3

Compact gain-saturated x-ray lasers down to 6.85 nm and amplification down to 5.85 nm²

3.1 Overview

This chapter presents results of experiments in which the Ti:Sapphire laser described in the last chapter is used to pump gain saturated lasers down to $\lambda = 6.85$ nm. Plasma-based x-ray lasers allow single-shot nano-scale imaging and other experiments requiring a large number of photons per pulse to be conducted in compact facilities. Previously, compact repetitively fired gain-saturated x-ray lasers have achieved wavelengths above $\lambda=8.85$ nm. The work in this thesis extended their range to $\lambda = 6.85$ nm by transient traveling wave excitation of Ni-like Gd ions in a plasma created with an optimized pre-pulse followed by rapid heating with an intense sub-ps pump pulse. Isoelectronic scaling also produced strong lasing at 6.67 nm and 6.11 nm in Ni-like Tb, and amplification at 6.41 nm and 5.85 nm in Ni-like Dy. This scaling to shorter wavelengths is obtained by progressively increasing the pump pulse grazing incidence angle to access increased plasma densities. We experimentally demonstrate that the optimum grazing incidence angle increases linearly with atomic number from 17 degrees for $Z=42$ (Mo) to 43 degrees for $Z=66$ (Dy). The results will enable applications of sub-7 nm lasers at compact facilities.

3.2 Introduction

The need for bright, energetic ultrafast x-ray laser pulses has motivated the commissioning of x-ray free electron lasers [1]. Alternatively, plasma-based x-ray lasers allow many experiments requiring bright, high energy, x-ray laser pulses to be conducted in compact facilities [2]–[6]. These lasers provide extremely monochromatic radiation, typically $\Delta \lambda / \lambda = 3 \times 10^{-5}$ [7], and

²A. Rockwood et al. "Compact gain-saturated x-ray lasers down to 6.85 nm and amplification down to 5.85 nm" *Optica* Vol. 5, Issue 3, pp. 257-262 (2018) © 2018 Optical Society of America

when injection-seeded can reach full spatial and temporal coherence [8]–[10]. The efficient generation of high energy x-ray laser pulses requires operation in the gain-saturated regime. In this regime stimulated emission can extract the majority of the energy stored in the population inversion [11]. Gain saturation in plasma-based x-ray lasers was demonstrated for wavelengths as short as 5.8 nm at large laser facilities [12], [13]. However, these results required pump pulse energies on target larger than 70 J, which limited the repetition rate to a few shots per hour. Alternatively, transient table-top lasers [14], [15] pumped by picosecond laser pulses at grazing incidence [16], [17] require much less energy and can operate at repetition rates of typically 5–10 Hz at wavelengths as short as 10.9 nm [18]. The repetition rate of these lasers was recently increased to 100 Hz using pump lasers pumped by laser diodes [19], and 400 Hz operation was very recently reported at $\lambda = 18.9$ nm in Ni-like Mo [20]. However, the extension of practical plasma-based x-ray lasers that can fire repetitively to sub-10 nm wavelengths is challenging. Alessi et al. used laser pump pulse energies of up to 7.5 J on target to extend table-top, repetitive 1 Hz transient collisional soft x-ray amplification down to 7.36 nm [21]. Nevertheless, gain saturated operation was limited to a shortest wavelength of 8.85 nm in Ni-like La. A more recent experiment conducted in Ni-like Sm using a Nd: glass pump laser capable of firing a shot every 25 minutes was reported to approach gain saturation [22]. However, this could not be verified due to large pulse-to-pulse output pulse energy variations and the low repetition rate of the pump laser. In the case of the 6.85 nm line of Ni-like Gd gain was observed in a plasma pumped by 250 J pulses, but the amplification was far from reaching gain saturation [23]. Alternatively, collisional recombination is being explored as a population inversion mechanism for transitions to the ground state to extend table top lasers to shorter wavelengths [24].

Here the extension of gain saturated compact repetitive x-ray lasers down to 6.85 nm (181 eV) in Ni-like Gd is described. Furthermore, in the same experiments we observed gain at even shorter wavelength transitions, down to 5.85 nm (212 eV) in Ni-like Dy. The experiments were performed with a pump laser capable of firing at repetition rates up to 3.3 Hz [25]. We also report measurements of the optimum grazing incidence pumping angle necessary for lasing at



figures/setup1.png

Figure 3.1: Solid rendering of the experimental setup for the pumping and measurement of the plasma based laser. Showing a normal pre-pulse followed by a short pumping pulse at a grazing incidence.

these wavelengths. The results reported here, in combination with previous measurements of the optimum angles for lasing in lower Z ions, allowed us to experimentally determine the optimum pump angle for laser operation at wavelengths between 18.9 nm and 5.85 nm. The results can be used to predict the optimum angles that will be required for lasing at shorter wavelengths.

3.3 Experimental set up and methods

The x-ray lasers were excited by irradiating 1-2 mm thick solid slab targets with a sequence of two laser pulses from a $\lambda = 800$ nm chirped pulse amplification Titanium:Sapphire (Ti:Sa) laser. The two pulse sequence consisted of a normal-incidence pre-pulse that ionizes the plasma to the vicinity of the Ni-like ionization stage, followed by a sub-picosecond pulse impinging at grazing incidence that rapidly heats the electrons to produce a transient population inversion by collisionally electron impact excitation. A depiction of the experimental setup is shown in Figure 3.1. The sub-picosecond pulse has a grazing incident angle of 35 degrees or 43 degrees for Sm and Gd respectively with a traveling-wave excitation velocity of $(1.0 \pm 0.03)c$. The pump laser has five Ti:Sa stages of amplification, of which the last three are pumped with the frequency-doubled output of high energy Nd:glass slab amplifiers that we have operated at repetition rates of up to 3.3 Hz [25]. An acousto-optic programmable dispersive filter was used after



Figure 3.2: Measured temporal profile of pre-pulse laser.



Figure 3.3: Measured spectrum of Ti:Sapphire with and with-out use of AOPDF to cut bandwidth.

the laser oscillator to tailor the bandwidth of the laser. This gives us the ability to adjust the length of the un-compressed pre-pulse from 45 ps to 300 ps to find the optimal conditions for laser amplification, which proved critical to obtain the results discussed below. Also, the intensity ratio of the pre-pulse to the sub-picosecond pulse was optimized using different beam splitters deflecting 30%, 40%, or 50% of the beam to be used as pre-pulse. Optimum pre-pulse plasma conditions were obtained using a 30% and 40% beam splitter to generate a pre-pulse with intensities of $I \sim 1.7 \times 10^{13} \text{ W/cm}^2$ and $2.5 \times 10^{13} \text{ W/cm}^2$ for Sm and Gd respectively with 185 ps duration. The pre-pulse temporal profile is shown in Figure 3.2. The chair shape comes from the use of the AOPDF (Dazzler) to cut the bandwidth of the stretched pulse. This cut results in the beginning wavelengths receiving larger gain and hence a larger amplitude. This is shown also by looking at the spectrum with and without the AOPDF as seen in Figure 3.3. By cutting the bandwidth we were able to adjust the pulse width of the pre-pulse. The pre-pulse was focused onto the target using the combination of a spherical and a cylindrical lens to form a line focus of approximately $15 \mu\text{m}$ FWHM width and 9 mm or 10 mm length for Sm and Gd respectively. To achieve efficient pumping by the sub-picosecond pulse, we developed a focusing geometry designed to create a plasma column of constant width along the target. This focusing method, consisting of two cylindrical mirrors, is the same we used previously to obtain gain-saturated lasing in Ni-Like La at 8.85 nm [22]. The plasma created by the pre-pulse is allowed to expand to reduce the density gradient and subsequently is rapidly heated with 7.1 J or 7.3 J pulse of a 0.7 ps FWHM duration for Sm and Gd respectively. This pump pulse is shaped into a line focus of approximately $30 \mu\text{m} \times 9 \text{ mm} - 10 \text{ mm}$ FWHM, corresponding to an intensity of $I \sim 3.5\text{-}3.7 \times 10^{15} \text{ W/cm}^2$ for Sm and Gd respectively. The target surface was tilted with respect to the axis of the sub-picosecond pulse to define a grazing incidence angle of 35 degrees or 43 degrees for efficient heating in the case of both Sm and Gd respectively. To optimize the incidence angle we changed the angle of the target respect to the short pulse beam and the position of the grating and CCD. Due to the short duration of the gain, the mismatch between the propagation velocities of the pump pulse and the amplified pulse significantly reduces the amplification of the x-ray laser

pulse. To overcome this limitation, a reflection echelon [15], [26] composed of six adjustable mirror segments was used to obtain traveling wave excitation. The traveling wave velocity was adjusted for each new angle, and the focus was corrected for each angle.

Gain measurements were conducted for both the Sm and Gd using single laser shots and moving the targets 1mm between shots. When the Gd laser was operated at 2.5-Hz repetition rate the target was translated at a speed of 2.5 mm s^{-1} to renew the surface after each shot. The output of the x-ray lasers was analyzed using a flat-field spectrometer with a nominally 1200-lines/mm variable space grating positioned at a grazing incidence angle of 3 degrees and a back-illuminated CCD detector placed at 48 cm from the target. Zirconium filters with a thickness of $2.0 \mu\text{m}$ were used in the Sm and Gd experiments for target lengths over 4 mm to avoid saturating the detector and to eliminate visible plasma light from reaching the detector. The filter thickness was reduced to $0.5 \mu\text{m}$ for the measurements with target lengths under 4 mm. In the case of Tb and Dy we used molybdenum filters with thicknesses of $0.6 \mu\text{m}$ and $0.3 \mu\text{m}$ respectively. The x-ray lasers pulse energies were estimated from the CCD counts taking into account the attenuation of the filters, the grating efficiency and the quantum efficiency of the detector.



Figure 3.4: End-on spectra showing the $\lambda = 7.36 \text{ nm}$, $4d^1 S_0-4p^1 P_1$ laser line of Ni-like Sm. Insert shows the spectra region near the $\lambda = 6.85 \text{ nm}$ laser line with scale multiplied by 10.



Figure 3.5: Measured $\lambda = 7.36$ nm laser intensity as a function of the pre-pulse duration. The points are the average of several laser shots and the error bar represents one standard deviation.



Figure 3.6: Measured laser intensity as a function of the delay between the peak of the pre-pulse and the peak of the short pulse. The plasma column length was 9 mm.

3.4 Results

Figure 3.4 shows a typical single shot spectra of the Ni-like Sm x-ray laser obtained created by depositing 7.1 J energy of sub-picosecond pulse and 4.3 J of pre-pulse energy on target.

Strong amplification is observed in the $4d^1 S_0-4p^1 P_1$ transition at $\lambda = 7.36$ nm (169 eV). The pre-pulse duration was optimized to maximize laser output. Figure 3.5 shows this was found to occur when the pre-pulse has a FWHM duration of ~ 185 ps. The delay between the pre-pulse and the sub-picosecond pulse controls the plasma density and density gradient in the gain region, as well as the degree of ionization (fraction of Ni-like ions) at the time of excitation by the sub-picosecond pulse. Figure 3.6 shows that the maximum laser output intensity is observed when the sub-picosecond pulse arrives at the target ~ 27 ps after the peak of the 185 ps FWHM pre-pulse. Figure 3.7 illustrates the Sm x-ray laser intensity grows by more than 3 orders of magnitude as the plasma column length increases from 3 mm to 8 mm. Saturation of the gain is observed to have an onset at a plasma-column length of approximately 5.5 mm. A fit of the data with an expression for the gain that takes into account saturation [27] yields a gain coefficient of 27.3 cm^{-1} with a gain-length product of 16.6. The energy of the most intense Sm laser pulses was estimated to be $\sim 1.8 \mu\text{J}$ from the CCD counts, a value that is sufficient to perform single shot imaging [28].



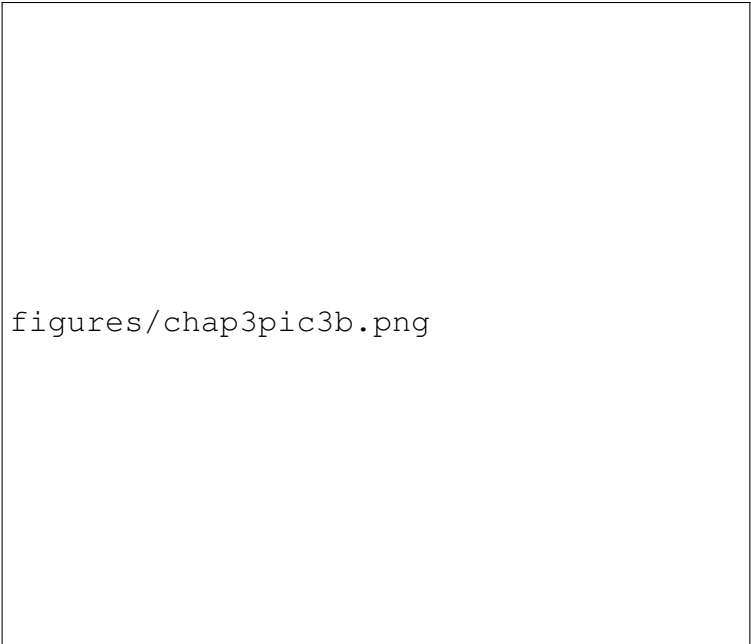
Figure 3.7: Intensity of the $\lambda = 7.36$ nm laser line of Ni-like Sm as a function of the plasma-column length. The red line is a fit of the data that yields a gain coefficient of 27.3 cm^{-1} and a gain-length product of 16.6. The error bar represents 1 standard deviation.

Similar pre-pulse and sub-picosecond pulse conditions were used to obtain a gain-saturated 6.85 nm (181 eV) laser in Ni-like Gd. Figure 3.8 shows a series of on-axis spectra as a function of the length for a Gd plasma column created by depositing 7.3 J of sub-picosecond pulse energy and 6.9 J of pre-pulse energy on a polished Gd slab target with other irradiation parameters similar to those described above. Figure 3.9 shows the increase in the $\lambda = 6.85$ nm laser line intensity as a function of plasma column length. A fit to the data gives a gain coefficient of 26.3 cm^{-1} and a gain length product of 16.2. The output pulse energy for the longest plasma column length is $\sim 1 \mu\text{J}$. Weak amplification was also observed for the $\lambda = 6.85$ nm line of Ni-like Sm (see Figure 3.8) and in the $\lambda = 6.33$ nm (196 eV) line of Ni-like Gd.



Figure 3.8: End-on spectra of a line-focus Gd plasma column showing saturated amplification in the $\lambda = 6.85$ nm line of Ni-like Gd. With the first two integrations plots on the right multiplied by 5.

The results were modeled and analyzed with hydrodynamic/atomic physics simulations conducted with the code Radex [29]. A post processor ray tracing code was used to model the soft x-ray laser beam propagation along the plasma column. This allowed us to compute the



figures/chap3pic3b.png

Figure 3.9: Intensity of the $\lambda = 6.85$ nm laser line as a function of the plasma-column length. The solid red line is a fit of the data that yields a gain coefficient of 26.3 cm^{-1} and a gain-length product of 16.2. The error bar represents 1 standard deviation. The black dashed line is the result of atomic physics/hydrodynamic simulation with a gain-length product of 16.9.

gain saturation behavior, the role of refraction, the x-ray laser output pulse energy and the beam divergence. To compute the small signal gain, the Ni-like ions were modeled with 287 levels including all inner and outer shell 314l and 315l levels, and 214l inner shell levels. Other ions in the vicinity of the Ni-like were modeled using 300 single and doubly excited levels using atomic data and collisional rates from the code HULLAC [30][3.30]. Ions far from the Ni-like state were modeled with just the lowest energy outer shell configuration plus the lowest inner shell and double excited levels. The atomic model was run self-consistently with the hydro code including up to 3000 levels. We observed that the computed gain decreases as the complexity of the atomic model and the number of levels is increased until the resulting gain becomes practically insensitive to a further increase in the number of levels. The dashed curve in Figure 3.9 is the result of the model simulations of the Gd 6.85 nm laser for the pump conditions used in the experiment assuming the width of the gain region in the direction parallel to the target is $10 \mu\text{m}$. Good agreement with the experimental results is observed. The model predicts a beam diver-

gence of 2.4 mrad in the directions parallel to the target, in good agreement with the measured value (Figure 3.10). The agreement with the experimental results allows us to use the simulations to further understand the operation of this x-ray laser amplifier. Figure 3.11 and Figure 3.12 shows the computed spatial distribution of the beam intensity as a function of plasma column length. The model simulations show that in the case of the higher Z-ions refraction shifts the maximum gain to the lower density region of $4 - 5 \times 10^{20} \text{ cm}^{-3}$. At this density the saturation intensity is computed to be $1.2 \times 10^{10} \text{ W/cm}^2$. Simulations show this intensity is reached after the rays travel $\sim 6 \text{ mm}$ along the plasma column axis. The output intensity is computed to exceed the saturation intensity by $> 3\times$ at the exit of the amplifier. Refraction is observed to shift the amplified beam progressively away from the target and to decrease the output pulse energy. In absence of refraction simulations predict the laser pulse energy would be five to ten times the amount with refraction, potentially reaching $>10\mu\text{J}$.



Figure 3.10: Measured (blue trace) and simulated (black dashed trace) Ni-like Gd laser far field beam intensity profile in the direction parallel to the target surface. The black dashed line is the modeled far field intensity, The FWHM beam divergence is $\sim 2.4 \text{ mrad}$.



figures/chap3pic5a.png

Figure 3.11: Computed evolution of the intensity distribution of the x-ray laser beam of the 6.85 nm line of Ni-like Gd as function of plasma column length. Intensity vs distance to the target for increasing plasma column lengths between 0.4 and 0.9 cm.

The demonstration of a gain-saturated tabletop laser at $\lambda = 6.85$ nm in Ni-like Gd at this reduced pump energy also opens the prospect for bright high-repetition-rate plasma-based lasers at shorter wavelengths. In progress toward this goal we made use of isoelectronic scaling along the elements of the lanthanide series to obtain lasing in several other shorter wavelength transitions from Ni-like ions. The spectra of Figure 3.13 show that the use of similar irradiation conditions for Ni-like Gd resulted in strong amplification in the $\lambda = 6.67$ nm (186 eV) and $\lambda = 6.11$ nm (203 eV) transitions of Ni-like Tb. Finally, we have also observed weak amplification in the $\lambda = 5.85$ nm (212 eV) and $\lambda = 6.41$ nm (193 eV) lines of Ni-like Dy (Figure 3.13) using the same pump conditions. The limited observed spread of the lines along the vertical direction in the detector, which length divergence (normal to the dispersion direction) is proportional to the divergence, shows a collimation that is a clear indication of amplification. Another evidence of amplification is the significant shot-to-shot variations of their intensity, indicative of exponential amplification

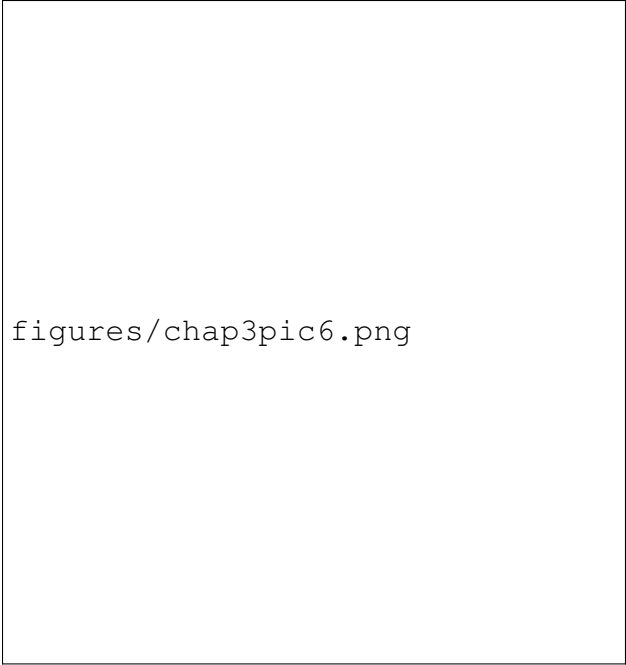


figures/chap3pic5b.png

Figure 3.12: Computed evolution of the intensity distribution of the x-ray laser beam of the 6.85 nm line of Ni-like Gd as function of plasma column length. Pseudocolor map of the laser line intensity as a function of distance to the target and plasma column length.

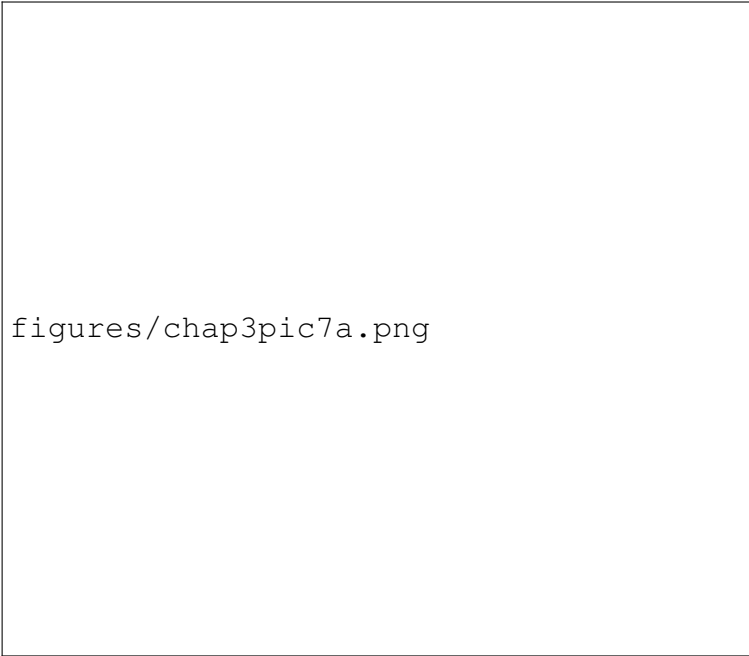
in the non-saturated regime. In all cases the traveling wave excitation was kept constant and near the speed of light in vacuum. The spectra in Figure 3.13 show that the intensity ratio of the longer wavelength to the shorter wavelength of the two $J=0-1$ lines becomes smaller as Z increases [31], with the shortest wavelength line becoming dominant for Ni-like Dy, as already observed in a normal incidence pumping experiment with much large laser pump energies [12], [32].

Another aspect of these amplifiers is the fact that collisional x-ray laser amplification at shorter wavelengths favors higher plasma densities. This is shown by the increase of the grazing incidence angle of the sub-picosecond pulse necessary for optimum laser amplification, which is related to the electron density at which the pump rays refract [33]. Combining the experimental data of optimum pump incidence angle obtained in this work to our previously published data for grazing incidence pumping for lasing in lower Z Ni-like ions [17], [18], [22], [34] it is possible to experimentally map the dependence of the optimum pump angle and plasma density for a large range of Z and lasing wavelengths. This provides both a bench mark for simulation codes, as well



figures/chap3pic6.png

Figure 3.13: End-on spectra showing lasing at progressively shorter wavelengths in the $4d^1 S_0$ - $4p^1 P_1$ line of nickel-like lanthanide ions, down to $\lambda = 5.85$ nm in nickel-like Dysprosium.



figures/chap3pic7a.png

Figure 3.14: Measured optimum grazing incidence angle as a function of atomic number. The dashed line is an extrapolation of the data.

as a prediction of the optimum condition for further scaling these lasers to shorter wavelengths. The increase in irradiation angle is observed to be linear over a broad range of atomic numbers

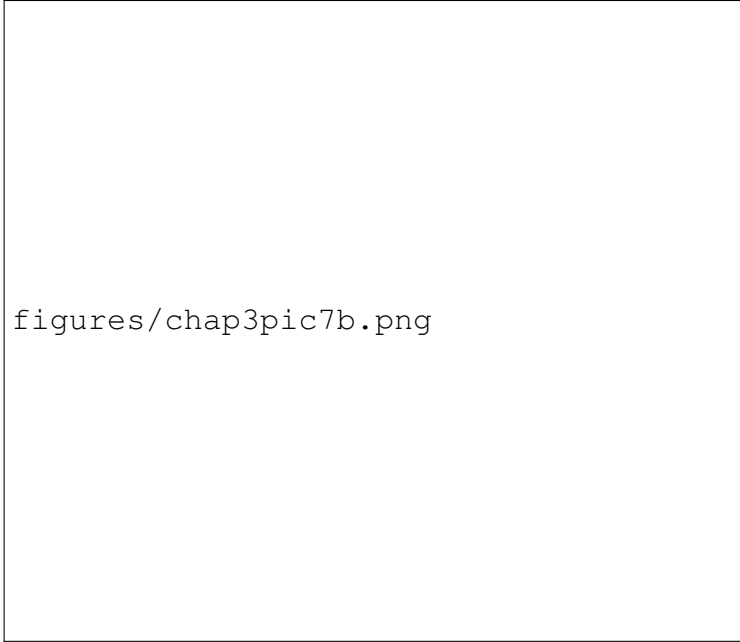


Figure 3.15: The optimum grazing incidence angle aextrapolation of the data.

ranging from $Z=42$ (Mo) to $Z=66$ (Dy) (Figure 3.14). In this range of Z the optimum picosecond or sub-picosecond pulse irradiation angle is observed to increase from a grazing incidence angle of ~ 17 degrees for Mo to 43 degrees for Dy. This corresponds to an increase in electron density from $1.5 \times 10^{20} \text{ cm}^{-3}$ to $8 \times 10^{20} \text{ cm}^{-3}$. As discussed above the model simulations show that in the case of the higher Z -ions refraction shifts the maximum gain to the lower density region.

3.5 Conclusion

In conclusion, we have extended compact gain-saturated plasma-based lasers to the shortest wavelength to date: 6.85 nm. We have also observed laser amplification in other Ni-like lanthanide ions at wavelengths as short as 5.85 nm, opening the possibility of scaling table-top gain saturated lasers to even shorter wavelengths. The optimum sub-picosecond pulse irradiation angle for the excitation of transient gain saturated Ni-like x-ray lasers was determined from experimental measurements to increase linearly for elements ranging from $Z = 42$ to $Z = 66$. The results will make possible applications requiring bright laser pulses with a large number of

photons at these short wavelengths, such as single shot ultra-high resolution imaging of dynamic nano-scale phenomena to be realized at compact facilities.

Bibliography

- [1] B. Mcneil and N. R. Thompson, “X-ray free-electron lasers,” *Nature Photonics*, vol. 4, Dec. 2010. DOI: 10.1038/nphoton.2010.239.
- [2] I. Kuznetsov, J. Filevich, F. Dong, M. Woolston, W. L. Chao, E. H. Anderson, E. R. Bernstein, D. C. Crick, J. J. Rocca, and C. S. Menoni, “Three-dimensional nanoscale molecular imaging by extreme ultraviolet laser ablation mass spectrometry,” in *Nature communications*, 2015.
- [3] G. Vaschenko, C. Brewer, F. Brizuela, Y. Wang, M. A. Larotonda, B. M. Luther, M. C. Marconi, J. J. Rocca, C. S. Menoni, E. H. Anderson, W. Chao, B. D. Harteneck, J. A. Liddle, Y. Liu, and D. T. Attwood, “Sub-38 nm resolution tabletop microscopy with 13 nm wavelength laser light,” *Opt. Lett.*, vol. 31, no. 9, pp. 1214–1216, May 2006. DOI: 10.1364/OL.31.001214. [Online]. Available: <http://ol.osa.org/abstract.cfm?URI=ol-31-9-1214>.
- [4] R. F Smith, J. Dunn, J. Nilsen, V. N Shlyaptsev, S. Moon, J. Filevich, J. J Rocca, M. C Marconi, J. R Hunter, and T. Barbee, “Picosecond x-ray laser interferometry of dense plasmas,” *Physical review letters*, vol. 89, p. 065 004, Sep. 2002. DOI: 10.1103/PhysRevLett.89.065004.
- [5] F. Brizuela, S. Carbajo, A. Sakdinawat, D. Alessi, D. H. Martz, Y. Wang, B. Luther, K. A. Goldberg, I. Mochi, D. T. Attwood, B. L. Fontaine, J. J. Rocca, and C. S. Menoni, “Extreme ultraviolet laser-based table-top aerial image metrology of lithographic masks,” *Opt. Express*, vol. 18, no. 14, pp. 14 467–14 473, Jul. 2010. DOI: 10.1364/OE.18.014467. [Online]. Available: <http://www.opticsexpress.org/abstract.cfm?URI=oe-18-14-14467>.
- [6] R. Z. Tai, K. Namikawa, M. Kishimoto, M. Tanaka, K. Sukegawa, N. Hasegawa, T. Kawachi, M. Kado, P. Lu, K. Nagashima, H. Daido, H. Maruyama, A. Sawada, M. Ando, and Y. Kato, “Picosecond Snapshot of the Speckles from Ferroelectric BaTiO₃ by Means of X-Ray Lasers,” *Physical Review Letters*, vol. 89, no. 25, 257602, p. 257 602, Dec. 2002. DOI: 10.1103/PhysRevLett.89.257602.

- [7] L. M. Meng, D. Alessi, O. Guilbaud, Y. Wang, M. Berrill, B. Luther, S. R. Domingue, D. H. Martz, D. Joyeux, S. D. Rossi, J. J. Rocca, and A. Klisnick, “Temporal coherence and spectral linewidth of an injection-seeded transient collisional soft x-ray laser,” *Opt. Express*, vol. 19, no. 13, pp. 12 087–12 092, Jun. 2011. DOI: 10.1364/OE.19.012087. [Online]. Available: <http://www.opticsexpress.org/abstract.cfm?URI=oe-19-13-12087>.
- [8] P. Zeitoun, G. Faivre, S. Sebban, J. Nejdil, A. Hallou, M. Fajardo, D. Aubert, P. Balcou, f. Burgy, D. Douillet, S. Kazamias, G. De Lacheze-Murel, T. Lefrou, S. Le Pape, P. Mercere, H. Merdji, A. S Morlens, J. P Rousseau, and C. Valentin, “A high-intensity highly coherent soft x-ray femtosecond laser seeded by a high harmonic beam,” *Nature*, vol. 431, pp. 426–9, Oct. 2004. DOI: 10.1038/nature02883.
- [9] Y. Wang, E. Granados, F. Pedaci, D. Alessi, B. Luther, M. Berrill, and J. J. Rocca, “Phase-coherent, injection-seeded, table-top soft-x-ray lasers at 18.9 nm and 13.9 nm,” *Nature Photonics*, vol. 2, pp. 94–98, Jan. 2008. DOI: 10.1038/nphoton.2007.280.
- [10] Y. Wang, L. Yin, S. Wang, M. C. Marconi, J. Dunn, E. Gullikson, and J. J. Rocca, “Single-shot soft x-ray laser linewidth measurement using a grating interferometer,” *Opt. Lett.*, vol. 38, no. 23, pp. 5004–5007, Dec. 2013. DOI: 10.1364/OL.38.005004. [Online]. Available: <http://ol.osa.org/abstract.cfm?URI=ol-38-23-5004>.
- [11] J. J. Rocca, “Table-top soft x-ray lasers,” *Review of Scientific Instruments*, vol. 70, no. 10, pp. 3799–3827, 1999. DOI: 10.1063/1.1150041. eprint: <https://doi.org/10.1063/1.1150041>. [Online]. Available: <https://doi.org/10.1063/1.1150041>.
- [12] R. Smith, G. J. Tallents, J. Zhang, G. Eker, S. McCabe, G. J. Pert, and E. Wolfrum, “Saturation behavior of two x-ray lasing transitions in Ni-like Dy,” vol. 59, R47–R50, Jan. 1999. DOI: 10.1103/PhysRevA.59.R47.
- [13] J. Zhang, A. G. MacPhee, J. Lin, E. Wolfrum, R. Smith, C. Danson, M. H. Key, C. L. S. Lewis, D. Neely, J. Nilsen, G. J. Pert, G. J. Tallents, and J. S. Wark, “A saturated x-ray laser beam at 7 nanometers,” *Science*, vol. 276, no. 5315, pp. 1097–1100, 1997, ISSN: 0036-8075.

- DOI: 10.1126/science.276.5315.1097. eprint: <http://science.sciencemag.org/content/276/5315/1097.full.pdf>. [Online]. Available: <http://science.sciencemag.org/content/276/5315/1097>.
- [14] P. Nickles, V. N. Shlyaptsev, M. Kalashnikov, M. Schnurer, I. Will, and W. Sandner, “Short pulse x-ray laser at 32.6 nm based on transient gain in ne-like titanium,” *Physical Review Letters - PHYS REV LETT*, vol. 78, pp. 2748–2751, Apr. 1997. DOI: 10.1103/PhysRevLett.78.2748.
- [15] J. Dunn, Y. Li, A. L. Osterheld, J. Nilsen, J. R. Hunter, and V. N. Shlyaptsev, “Gain saturation regime for laser-driven tabletop, transient ni-like ion x-ray lasers,” *Phys. Rev. Lett.*, vol. 84, pp. 4834–4837, 21 May 2000. DOI: 10.1103/PhysRevLett.84.4834. [Online]. Available: <https://link.aps.org/doi/10.1103/PhysRevLett.84.4834>.
- [16] R. Keenan, J. Dunn, P. K. Patel, D. F. Price, R. F. Smith, and V. N. Shlyaptsev, “High-repetition-rate grazing-incidence pumped x-ray laser operating at 18.9 nm,” *Phys. Rev. Lett.*, vol. 94, p. 103901, 10 Mar. 2005. DOI: 10.1103/PhysRevLett.94.103901. [Online]. Available: <https://link.aps.org/doi/10.1103/PhysRevLett.94.103901>.
- [17] B. Luther, Y. Wang, M. Larotonda, D. Alessi, M. Berrill, M. C Marconi, J. J Rocca, and V. N Shlyaptsev, “Saturated high-repetition-rate 18.9-nm tabletop laser in nickellike molybdenum,” *Optics letters*, vol. 30, pp. 165–7, Feb. 2005. DOI: 10.1364/OL.30.000165.
- [18] Y. Wang, M. A. Larotonda, B. M. Luther, D. Alessi, M. Berrill, V. N. Shlyaptsev, and J. J. Rocca, “Demonstration of high-repetition-rate tabletop soft-x-ray lasers with saturated output at wavelengths down to 13.9 nm and gain down to 10.9 nm,” vol. 72, no. 5, 053807, p. 053 807, Nov. 2005. DOI: 10.1103/PhysRevA.72.053807.
- [19] B. A. Reagan, M. Berrill, K. A. Wernsing, C. Baumgarten, M. Woolston, and J. J. Rocca, “High-average-power, 100-hz-repetition-rate, tabletop soft-x-ray lasers at sub-15-nm wavelengths,” *Phys. Rev. A*, vol. 89, p. 053 820, 5 May 2014. DOI: 10.1103/PhysRevA.89.053820. [Online]. Available: <https://link.aps.org/doi/10.1103/PhysRevA.89.053820>.

- [20] C. Baumgarten, M. Pedicone, H. Bravo, H. Wang, L. Yin, C. S. Menoni, J. J. Rocca, and B. A. Reagan, “1 j, 0.5 khz repetition rate picosecond laser,” *Opt. Lett.*, vol. 41, no. 14, pp. 3339–3342, Jul. 2016. DOI: 10.1364/OL.41.003339. [Online]. Available: <http://ol.osa.org/abstract.cfm?URI=ol-41-14-3339>.
- [21] D. Alessi, Y. Wang, B. Luther, L. Yin, D. Martz, M. Woolston, Y. Liu, M. Berrill, and R. Jorge, “Efficient excitation of gain-saturated sub9-nm-wavelength tabletop soft-x-ray lasers and lasing down to 7.36 nm,” *Physical Review X*, vol. 1, Dec. 2011. DOI: 10.1103/PhysRevX.1.021023.
- [22] J. Balmer and F. Staub F.and Jia, *X-Ray Lasers 2012*. Springer Proceedings in Physics, Paris, 2014, vol. vol 147 Chap. 5.
- [23] H. Daido, Y. Kato, K. Murai, S. Ninomiya, R. Kodama, G. Yuan, Y. Oshikane, M. Takagi, H. Takabe, and F. Koike, “Efficient soft x-ray lasing at 6 to 8 nm with nickel-like lanthanide ions,” *Phys. Rev. Lett.*, vol. 75, pp. 1074–1077, 6 Aug. 1995. DOI: 10.1103/PhysRevLett.75.1074. [Online]. Available: <https://link.aps.org/doi/10.1103/PhysRevLett.75.1074>.
- [24] Y. Luo, A. Morozov, D. Gordon, P. Sprangle, A. Svidzinsky, H. Xia, M. Scully, and S. Suckewer, “Possibility of Recombination Gain Increase in CV Ions at 4.0 nm Via Coherence,” in *X-Ray Lasers 2014, Springer Proceedings in Physics, Volume 169. ISBN 978-3-319-19520-9. Springer International Publishing Switzerland, 2016, p. 21*, J. Rocca, C. Menoni, and M. Marconi, Eds., 2016, p. 21. DOI: 10.1007/978-3-319-19521-6_3.
- [25] Y. Wang, S. Wang, A. Rockwood, B. M. Luther, R. Hollinger, A. Curtis, C. Calvi, C. S. Menoni, and J. J. Rocca, “0.85 pw laser operation at 3.3 hz and high-contrast ultrahigh-intensity $\lambda = 400$ nm second-harmonic beamline,” *Opt. Lett.*, vol. 42, no. 19, pp. 3828–3831, Oct. 2017. DOI: 10.1364/OL.42.003828. [Online]. Available: <http://ol.osa.org/abstract.cfm?URI=ol-42-19-3828>.

- [26] J. Crespo Lopez-Urrutia, E. E. Fill, W. Theobald, and C. Wuelker, “Traveling-wave excitation of an x-ray laser medium,” *Proc SPIE*, pp. 258–264, Feb. 1994. DOI: 10.1117/12.167393.
- [27] G. J. Tallents, Y. Abou-Ali, M. Edwards, R. E. King, G. J. Pert, S. J. Pestehe, F. Strati, R. Keenan, C. L. S. Lewis, S. Topping, O. Guilbaud, A. Klisnick, D. Ros, R. Clarke, D. Neely, and M. Notley, “Saturated and short pulse duration x-ray lasers,” *AIP Conference Proceedings*, vol. 641, no. 1, pp. 291–297, 2002. DOI: 10.1063/1.1521033. eprint: <https://aip.scitation.org/doi/pdf/10.1063/1.1521033>. [Online]. Available: <https://aip.scitation.org/doi/abs/10.1063/1.1521033>.
- [28] M.-C. Chou, R.-P. Huang, P.-H. Lin, C.-T. Huang, S.-y. Chen, H.-H. Chu, J. Wang, and J.-Y. Lin, “Single-shot soft-x-ray digital holographic microscopy with an adjustable field of view and magnification,” *Opt. Lett.*, vol. 34, no. 5, pp. 623–625, Mar. 2009. DOI: 10.1364/OL.34.000623. [Online]. Available: <http://ol.osa.org/abstract.cfm?URI=ol-34-5-623>.
- [29] A. Vinogradov and V. N Shlyaptsev, “Characteristics of a laser plasma x-ray source (review),” *Soviet Journal of Quantum Electronics*, vol. 17, p. 1, Oct. 2007. DOI: 10.1070/QE1987v017n01ABEH006346.
- [30] A. Bar-Shalom, M. Klapisch, and J. Oreg, “Hullac, an integrated computer package for atomic processes in plasmas,” *Journal of Quantitative Spectroscopy and Radiative Transfer*, vol. 71, pp. 169–188, Oct. 2001. DOI: 10.1016/S0022-4073(01)00066-8.
- [31] H. Daido, “Review of soft x-ray laser researches and developments,” *Reports on Progress in Physics*, vol. 65, p. 1513, Sep. 2002. DOI: 10.1088/0034-4885/65/10/204.
- [32] B. J. MacGowan, L. B. Da Silva, D. J. Fields, C. J. Keane, J. A. Koch, R. A. London, D. L. Matthews, S. Maxon, S. Mrowka, A. L. Osterheld, J. H. Scofield, G. Shimkaveg, J. E. Trebes, and R. S. Walling, “Short wavelength x-ray laser research at the lawrence livermore national laboratory,” *Physics of Fluids B: Plasma Physics*, vol. 4, no. 7, pp. 2326–2337,

1992. DOI: 10.1063/1.860203. eprint: <https://doi.org/10.1063/1.860203>. [Online]. Available: <https://doi.org/10.1063/1.860203>.
- [33] R. A. London, “Beam optics of exploding foil plasma x-ray lasers,” *The Physics of Fluids*, vol. 31, no. 1, pp. 184–192, 1988. DOI: 10.1063/1.866565. eprint: <https://aip.scitation.org/doi/pdf/10.1063/1.866565>. [Online]. Available: <https://aip.scitation.org/doi/abs/10.1063/1.866565>.
- [34] M. A. Larotonda, B. M. Luther, Y. Wang, Y. Liu, D. Alessi, M. Berrill, A. Dummer, F. Brizuela, C. S. Menoni, M. C. Marconi, V. N. Shlyaptsev, J. Dunn, and J. J. Rocca, “Characteristics of a saturated 18.9-nm tabletop laser operating at 5-hz repetition rate,” *IEEE Journal of Selected Topics in Quantum Electronics*, vol. 10, no. 6, pp. 1363–1367, Nov. 2004, ISSN: 1077-260X. DOI: 10.1109/JSTQE.2004.838038.

Chapter 4

Single shot, large field of view, Fourier transform holography with 5 ps resolution using an 18.9 nm laser

4.1 Overview

This chapter discusses the demonstration of single shot Fourier transform holography with a temporal resolution of 5 ps realized using a plasma based highly coherent Ni-like molybdenum SXR laser at 18.9 nm. The SXR laser is pumped by the Ti:Sapphire laser described in Chapter 2. To achieve the high spatial coherence necessary for holography, the SRX source is implemented using a dual-plasma scheme in which a small fraction of the wavefront generated from a first SXR laser plasma amplifier is injected in a second plasma amplifier to provide a fully spatially coherent seed. silver nano-wires 200 nm in diameter were imaged over a 7 μm diameter field of view utilizing a reference beam focused through a 3 μm hole by a 200 nm outer zone free standing zone plate (ZP). The final acquired image is numerically reconstructed by 2D Fourier transform. The 10%– 90% knife edge spatial resolution is measured to be 62 nm.

4.2 Introduction

High-resolution imaging is an important diagnostic tool in fundamental science and technology. The use of photons in place of electrons for imaging in the nano-scale provides higher penetration depth, chemical sensitivity and simpler sample preparation [1], [2]. The achievable spatial resolution r scales linearly with the wavelength [3]

$$r = 0.61\lambda/NA \tag{4.1}$$

NA is the numerical aperture and λ is the wavelength. Because of its short wavelength range, SXR light enables the opportunity to achieve very high spatial resolution. However, one of the main limitations in implementing high resolution SXR imaging is adequate optics for imaging and/or focusing the beams [4]–[6]. At SXR wavelengths compensating for aberrations typically present in zone plates used to focus the beams is a difficult task. This will be discussed later on in this chapter. Alternative imaging techniques that get around this problem are based on eliminating the optics all together and measuring the SXR scattered light directly. By measuring the scatter light and using phase retrieval algorithms it is possible to calculate the missing phase information [7]. One such technique is known as coherent diffractive imaging (CDI). CDI uses phase retrieval algorithms taking advantage of all the known information to numerically reconstruct the image from the far field diffraction pattern. Potential limitations of this technique are that results are heavily dependent on recording parameters such as the linearity of the detector, the spatial coherence of the source, and its bandwidth that determines the temporal coherence, the ratio of oversampling and the signal-to-noise ratio in the measured data [8], [9]. Using CDI in both 2-D and 3-D, resolutions of ~ 5 nm were achieved [10], [11] using an undulator beamline and a free-electron laser (FEL) respectively. High photon flux is critical to achieve this resolution. CDI have been used to perform high resolution imaging in a variety of fields including imaging the modern semiconductor integrated circuits and it's complete 3D structure [12], investigate biological nano-scale structures [13], and mapping the chemical composition in the study of delithiation in a nanoplate of LiFePO_4 [10]. Resolutions as high as 13 nm have been obtained using table top sources[14], [15]. By using picosecond and femtosecond pulses in pump-probe experiments, fast processes have been studied [16], [17]

An alternative approach of Fourier transform holography (FTH) is utilized in this work. In FTH the reference beam is a point source. Retrieval of the object wave intensity and phase is achieved by computing the 2 dimensional Fourier transform of the recorded hologram. Reconstructing the image is very fast and robust. There are several factors that determine the achievable spatial resolution and field of view. Because the reconstruction of the image is obtained

by a convolution with the reference point source, the spatial resolution is related to the size of this reference source. On the other hand, the field of view is directly linked to the spatial and temporal coherence of the laser used for the recording. Other experimental parameters like the numerical aperture and the detector pixel size limits the maximum spatial frequency that can be recorded and consequently sets a limit on the spatial resolution [18], [19]. In most of the FTH experiments the reference point source is obtained illuminating a small pinhole located in the same plane as the object. Because the spatial resolution is directly related to its size, a simple strategy to improve the resolution is to reduce the diameter of the pinhole. However, this decreases the intensity of the reference beam. The consequence is that it becomes hard to obtain good visibility interference fringes because the reference and the object beams have very dissimilar intensities.

Previous work at synchrotrons produced half-pitch resolutions of ~ 50 nm using Fourier transform holography (FTH). The reference structure was the limiting factor. [20], [21]. The FTH imaging method with x-ray pulses from a FEL with femtosecond temporal resolution produced groundbreaking studies of ultrafast magnetism [17], [22]. Looking at SXR imaging outside FEL and synchrotrons, in 2009 the highest resolution obtained was 53 nm in an experiment which used a high harmonic source. The acquisition time was in the range of hours [23]. In 2018, FTH using a high harmonic source achieved a half-pitch resolution of 34 nm with a much reduced exposure time of only tens of seconds. This experiment was in the transmission geometry and had a 50 nm reference hole for the spherical wave[24]. In 2010, using a single shot plasma based SXR laser, a resolution of 87nm was obtained[25]. In these experiments, a resolution beyond the size of the reference hole was made possible by the use of multiple reference holes that create multiple images that were processed with iterative phase retrieval imaging algorithms. In the FTH experiments mentioned in [25] a resolution of 87nm with a single shot was reached. The area imaged was limited to $3\mu m$ by $3\mu m$ ($9\mu m^2$) in which half the area was opaque. This was mostly limited by the insufficient amount of light that passed through the reference pinholes compared to the amount that was transmitted through the sample. In the work by G. K. Tadesse et al. [24]] who obtained 34 nm resolution, the imaged object area was $0.075\mu m^2$.

In the work performed as part of this dissertation, we followed an alternative approach. Instead of using a single or multiple pinhole as the point reference source, we used a custom made Fresnel zone plate consisting of a zone plate with a central aperture. This special zone plate played the role of a beam splitter, generating the point source for the reference through the focal point formed by the periphery of the zone plate, while the object beam was transmitted through the central opening. This experimental setup was used before with a synchrotron source to image magnetic materials [26]. In our experiment we were able to achieve a resolution of up to 62nm with a single shot SRX laser illumination, yielding a simultaneous temporal resolution of 5 ps. The utilization of the zone plate with a central aperture has the immediate consequence to increase the amount of light in the reference source by orders of magnitude and therefore increases the area of the object by equalizing the intensities of the object and reference beams. In the experiment presented here the area imaged was $38.5 \mu m^2$ or 8.5 times in Ref.[25] and 500 times the area in Ref. [24]. By controlling the axial position of the ZP it is possible to control the focal plane of the reconstructed image to places other than the plane directly on the substrate. This is discussed in more detail in section 4.3.2.

4.3 Experimental Setup

Figure 4.1 shows a diagram of the experimental setup. An incoming coherent SXR laser impinges on a custom made ZP that is used as a beam splitter. The central aperture of the ZP allows the incoming beam to illuminate an object area located in a second plane downstream. The remaining part of the beam that impinges in the periphery of the ZP is focused into a focal point placed in the same plane as the object. The scattered beam in the object and this reference beam interfere and the resulting fringes are recorded on a CCD. The interference pattern constitutes a hologram that can be rapidly processed to produce a reconstructed image. This setup for producing the hologram is capable of recording holographic images with a temporal resolution given by the pulse-width of the illuminating laser (5 ps) and a spatial resolution given by the focus spot size of the ZP.



Figure 4.1: (a) Depiction of the Fourier holography setup with zone plate and sample with the two holes followed by a CCD. (b) Zoom in of the sample and the different SRX laser beams in the setup.

4.3.1 Highly coherent SXR laser

The implementation of soft x-ray FTH requires of a coherent soft x-ray source. Recently, laser driven HHG sources with a photon flux up to 10^{14} photons/second have been demonstrated [27]–[29]. However these sources are limited in the energy per pulse, that is typically in the

order of 2×10^9 photons for a wavelength of 57 nm [27], 10^7 photons for a wavelength of 31 nm [27] and 2×10^4 photons for a wavelength of 10 nm [28]. [18]. On the other hand, plasma based SXR lasers deliver orders of magnitude more photons per pulse. In the case of the laser source used in this experiment $\sim 2 \times 10^{11}$ photons per shot at wavelengths of 18.9 nm, which makes it a better fit for single shot imaging experiments. plasma based lasers have been used for conventional microscopy with spatial resolutions down to 38 nm using a 13 nm wavelength laser [30]. Gabor holography with a resolution of 46 nm has been demonstrated with a SXR plasma based laser at 46.9 nm [31].

In a soft x-ray laser that operates in the ASE regime a spatially coherent SXR beam may be generated by amplification in a gain medium with the Fresnel number $N < 1$ [32], where $N = a^2 / f \lambda_L$ in which a and f are the radius and length of the amplifier, respectively and λ_L is the laser wavelength. In earlier plasma-based lasers, this condition was not satisfied even though the effective gain length was increased by double-pass amplification [33]–[35]. Even with multipass amplification [36], which sufficiently fulfilled this condition, the spatial coherence has not significantly improved. Another factor that limits the spatial coherence is the large gradient in the refraction index that appear in the gain medium plasma, discussed in Chapter 1. Attempts to compensate the x-ray refraction using curved targets [37] has also not been sufficient to significantly improve the coherence. To achieve the spatial coherence necessary for holographic recording we used a SXR laser scheme with two plasma amplifiers located in the same axis as shown schematically in Figure 4.2. The first plasma amplifier acts as the seed, producing a laser beam that is spatially filtered by the second amplifier column. The technique of a double plasma amplifier to improve the spatial coherence of the SXR laser was first demonstrated by M. Nishikino et al. [38]. In our experiment the seed and the amplifier plasma columns were separated by 24.5 mm. This distance assures that only a small fraction of the seed wavefront is further amplified, allowing for a high spatial coherence amplified beam due to spatial filtering.

The SXR laser used in this experiment made use of a 18.9 nm Mo+18 plasma amplifier both for the seed and the booster amplifier columns. The two amplifier columns were pumped with

an adequate delay so the seed laser would see a peak amplification when traveling through at the booster amplifier column. The coherence resulting from the two-stage amplifier scheme was measured using a Young's double slit experiment. The beam was sent through two slits intersecting the far sides of the beam and the interference pattern was detected in a CCD. The results from this measurement are shown in Figure 4.3. The spatial coherence is directly related to the fringe visibility [39]. The high contrast in the interference fringes obtained in our experiment shown in Figure 4.3 is the signature of a practically fully transverse coherent beam.

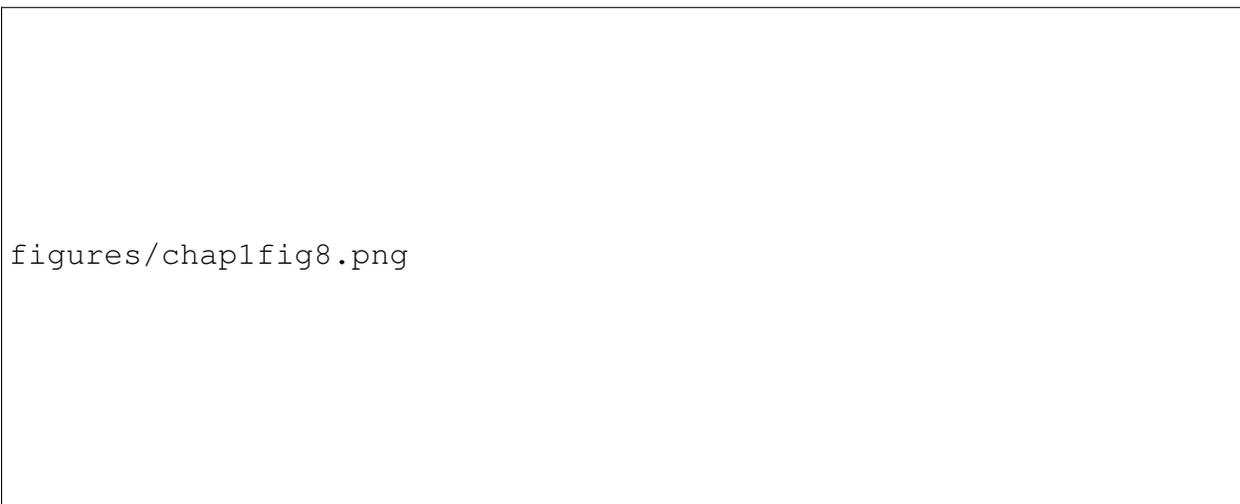
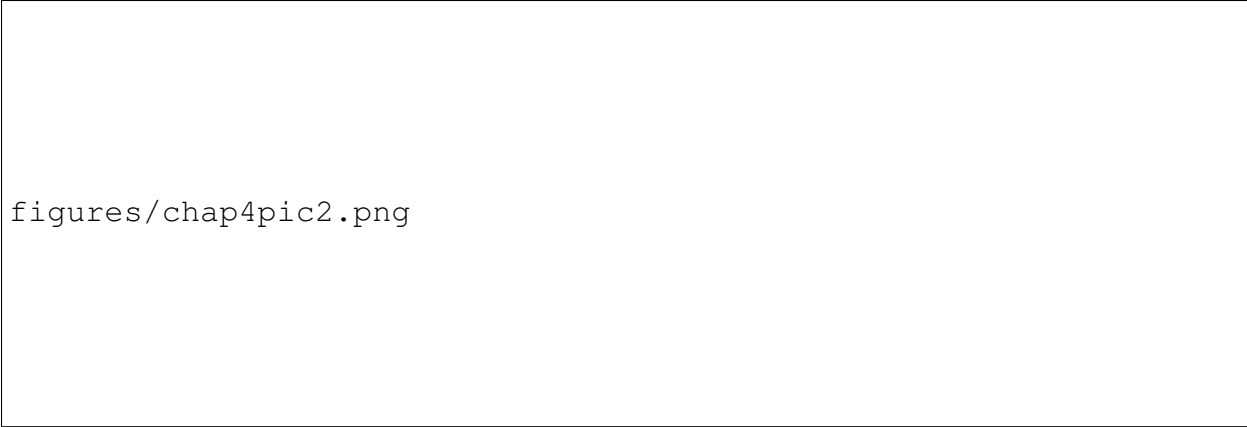


Figure 4.2: Depiction of the seed and amplifier setup used by CSU to create spatially coherent SXR beam.

This seed amplifier SRX laser configuration also improves the beam divergence as discussed in Chapter 1 and shown in Figure 4.4. In Figure 4.4(a) a typical SXR laser shot from the first plasma amplifier shows a divergence of the order of 5 mrad. Adding the second plasma amplifier automatically improved the divergence, because only a small portion of the beam is further amplified yielding to a lower divergence (1 mrad) and a high spatial coherence (Figure 4.4(b)). The use of the seed-amplifier configuration gives us an 18.9 nm laser with good spatial coherence, a pulse duration of 5 ps and a low diverge beam that allow us to concentrate the energy in a small area



figures/chap4pic2.png

Figure 4.3: Dual molybdenum amplifier SXR 18.9nm beam after passing through a double slit showing interference and good spatial coherence.



figures/chap1fig9a.png

(a)



figures/chap1fig9b.png

(b)

Figure 4.4: (a) Unseeded Ni-like Mo 18.9nm SXR laser in the far field. The sharp line comes from the second amplifiers shadow. (b) Seeded Ni-like Mo 18.9nm SXR laser in the far field. The intensities in color of the two images are not normalized because if they were you would have a difficult time seeing the unseeded beam as it is several times weaker.

4.3.2 Zone Plate

In the FTH setup that we used in this work, the reference and illumination beams were produced by a ZP that is used as a beamsplitter. The reference beam came from the 3rd order diffracted beam that produces a focal point that constitutes a spherically diverging beam after the focus. This focus is sent through a pin-hole with a diameter of $3 \mu\text{m}$. The pin-hole serves the purpose to block the other orders produced by the ZP that would blur the interference pattern.

The sample is illuminated by the light that passes through the central hole $30 \mu\text{m}$ in diameter in the ZP.

The object beam and the spherical reference beam interfere to produce the interference pattern which is stored in the CCD camera as a hologram. The reconstruction of the hologram is performed by an FFT operation, that produces an image of the object at the same plane where the reference source was located. This property allows for the inspection of the object at different planes along the optical axis by displacing the ZP. Using a ZP to generate the point reference beam serves two purposes. Firstly, gathers a larger fraction of the illuminating beam is gathered. This allows for a better intensity equalization between the object and the reference beams. Secondly, a small focal point is obtained that serves as the point source. A scheme of a ZP and the different order focuses is shown in Figure 4.5. For a ZP the achievable spot size ratios follows the equation that is directly related to the Rayleigh resolution.

$$r_{null} = \frac{0.610\lambda}{NA n_{order}} = \Delta r_{Rayl} \quad (4.2)$$

By substituting $NA \simeq \frac{\lambda}{2\Delta r}$ where Δr is the outer zone width spacing we get an achievable resolution of.

$$\Delta r_{Rayl} = \frac{1.22\Delta r}{n_{order}} \quad (4.3)$$

From equation (4.3) it is clear that to use a higher order on the ZP can obtain a higher resolution. However, the drawback is the diffraction efficiency of the ZP decreases with the order number. In a self standing ZP, half the incident light is lost due to absorption. The 0^{th} order has about 25% of the incident light, the 1^{st} and -1^{st} orders has around 10% of the light each while the 3^{rd} order has around 1% of the incident light on the ZP [3]. Higher orders will have even an lower fraction of the available incident beam.

In our experiment we found that the 3^{rd} order from the ZP had an adequate intensity to achieve good visibility fringes. The ZP we used was a free standing 0.5 mm outer diameter

ZP with an outer zone width of 200 nm and an inner hole with a diameter of 30 μm . This ZP was originally made for a 46.9 nm laser and to be used in the 1st order. The ZP was made by Lawrence Berkeley National Laboratory's Materials Sciences Division. The 3rd order focal point has a calculated spot size of 81 nm.

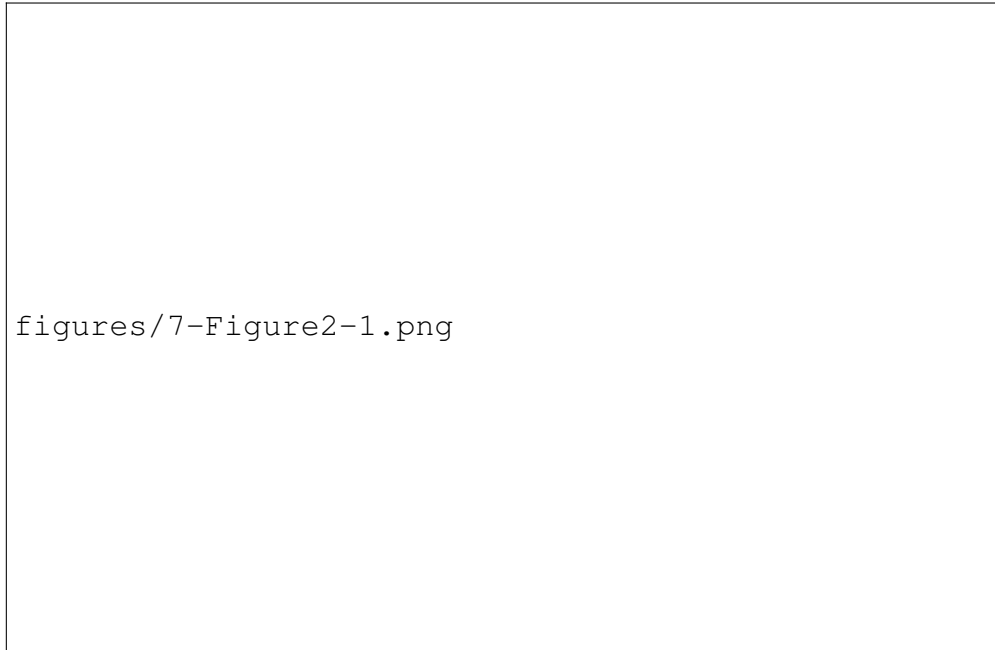


Figure 4.5: Depiction of a zone plate and the different order focus and directions. (from [40]).

4.3.3 Sample holder and CCD

The object we used consisted of an ensemble of 200 nm in diameter silver nano-wires that were randomly placed on a sample holder. The sample holder was composed of a 50nm thick Si_2N_3 membrane coated with 5nm Cr and 30nm Au layers to enhance the absorption. In the opaque membrane a 7 μm diameter region was left without the Cr and Au coatings producing a regions with higher transmission (approximately 57%) for the laser beam. This circular region defined by lithography plays the role of the sample holder. Additionally a 3 μm hole was defined in the membrane to allow for the passage of the reference beam produced by the 3rd order focus of the ZP. The pinhole for the reference beam was located 8 μm from sample hole as shown

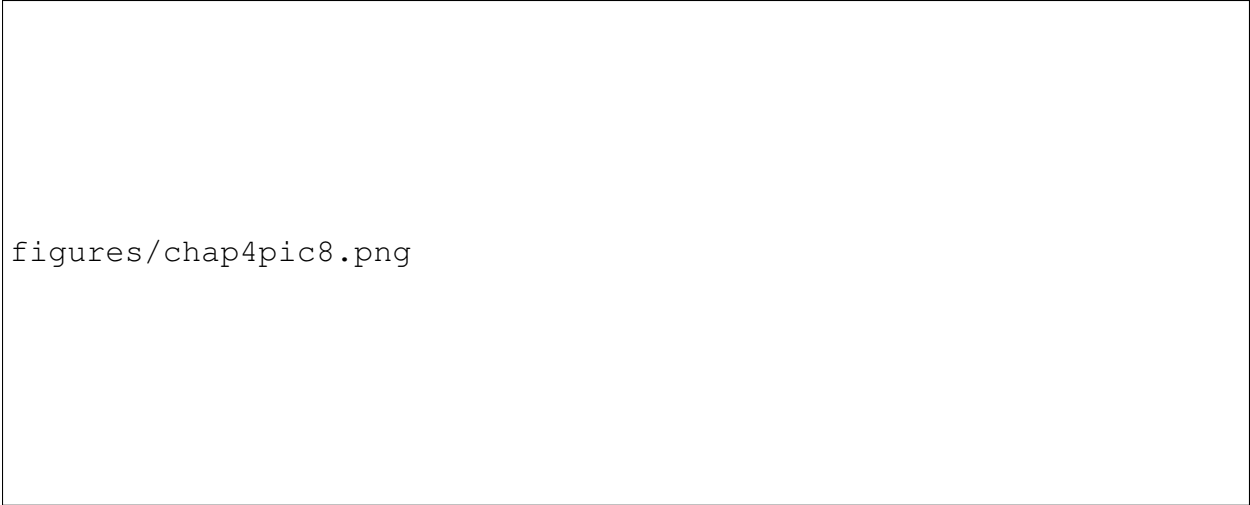
in Figure 4.6. The Ag nano-wires were spin coated on top of the sample holder membranes in such a way that some nano-wires were randomly deposited on top of the larger ($7 \mu\text{m}$) high transmission region. Two different samples were prepared following this protocol. Scanning electron microscope images of the two samples are shown in Figure 4.6.

Maximizing the useful field of view

The imaged area was maximized under the following constraints: The minimum distance between the two holes has to be more than the diameter of the large hole. This is to fulfill the separation criterion. In the FFT reconstruction process, the central part of the image corresponds to the autocorrelation of the object wave. The useful image is obtained by the correlation between the object wave and the point reference wave, that has to be separated from the optical axis at least by a distance equal to the diameter of the object wave in order to not get merged with the autocorrelation signal. This can be seen by the bright area in the middle of Figure 4.8(a). The sample high transmission region also needs to be illuminated with the light traveling through the central opening of the ZP. This makes the maximum distance from the reference hole $15 \mu\text{m}$ which leaves a distance of $7 \mu\text{m}$ for a sample area. The distance between the reference hole and the sample also determines the spatial frequency of the interference fringes. Since a pixelated CCD is used to record the hologram the size of the detector's pixels limits the minimum interference fringe size to two pixels in order to record the interference without aliasing.

4.4 Results

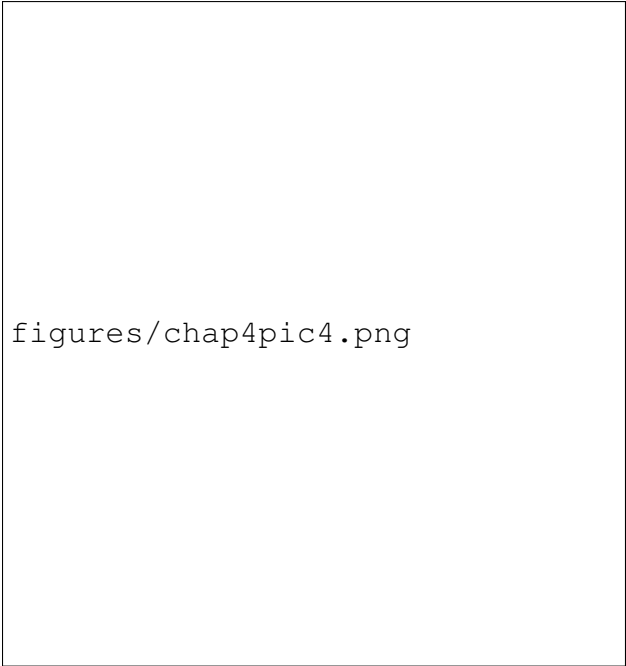
A typical hologram is shown in Figure 4.7. The raw data was further processed before applying the FFT in order to improve the image quality after the final reconstruction. The hologram was multiplied by a mask to zero out the regions of outside the zone with interference fringes to reduce the influence of the noise. Performing a fast Fourier transform (FFT) on the data finally resulted in an image in the object at the plane of the ZP focus. This is shown in Figure 4.8. By zooming in on the area of interest the nano-wires are clearly visible. The two samples were



figures/chap4pic8.png

Figure 4.6: Electron microscope image of two samples used in this work. Each sample has a $7 \mu m$ hole with 200 nm silver nanowires over it and a $3 \mu m$ hole separated by $11 \mu m$.

imaged using a SEM to have a reference to compare with the holographic images. Both, SEM and holograms, are shown in Figure 4.9



figures/chap4pic4.png

Figure 4.7: Typical single shot SXR Fourier holography image taken with a zoom of the fringe pattern.

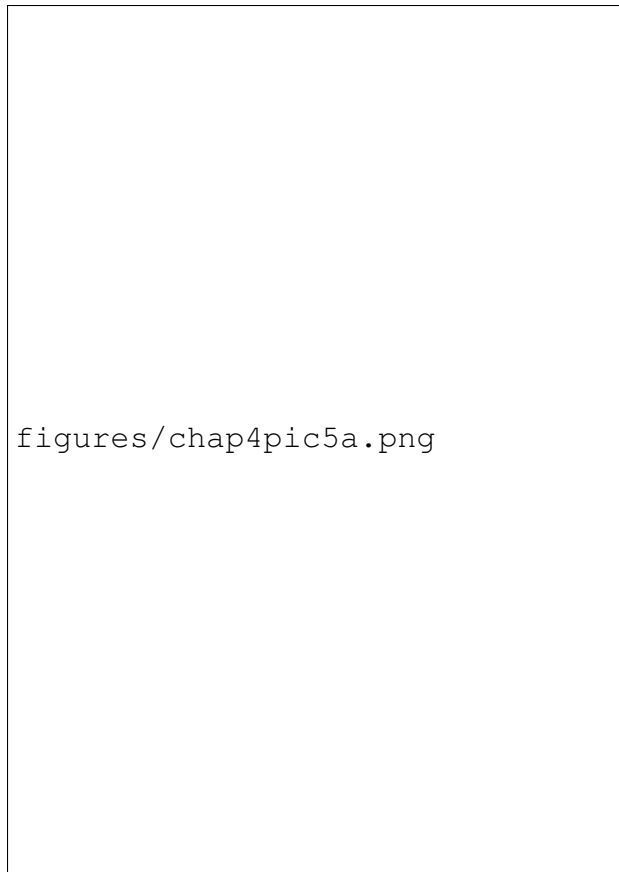


Figure 4.8: (a) The Fourier transform of the hologram (b) A zoom of the section showing the sample and the 200nm silver nano-wires.

The resolution was measured to be 62 nm using the 10% to 90% knife edge criterion [41]. One typical cross section of the image is shown in Figure 4.10, with a small red segment indicating the region where the cut was performed in the reconstructed image.

The utilization of the ZP to implement the point reference source allowed for an extended field of view of $38.5 \mu m^2$. This area is up to 500 times larger than former reported work[24], [25]. This is a significant improvement that increase the possibilities of SXR FTH for practical nanoscale imaging applications. Even with small modifications to this set up it is possible to increase the imaging area to $241 \mu m^2$. This is accomplished by increasing the high transmission region to a half doughnut shaped design instead of the circle. This would utilise all the area that is illuminated by the central opening in the ZP. The area could also be larger by increasing the size of the central opening on the ZP making the illuminated area larger. This method with its



figures/chap4pic7.png

Figure 4.9: Electron microscope image (left) and single shot holographic images (right) of the 200 nm silver nanowires over a $7\ \mu\text{m}$ hole.

advantages of high spatial and temporal resolution makes many imaging opportunities possible, including the imaging of sub-nanosecond scale nanoscale dynamic phenomena.

4.5 How to further improve resolution in future work

We demonstrated 62 nm spatial resolution with Fourier transform holography obtained using a single shot 5 ps highly coherent SXR laser operated at a wavelength of 18.9 nm. We also have a imaging field of view of $38.5\ \mu\text{m}^2$ that is dramatically larger than other methods used in this



Figure 4.10: a) A 10% to 90% characteristic knife edge cut of the image showing a spatial resolution of 62 nm. With the reconstructed data as red circles and the polynomial fit as a blue line. b) The reconstructed image showing the cut area in red.

field in the past. The results presented here improve the temporal resolution to the picosecond range. With the progress in shorter wavelength SXR plasma lasers one will be able to continue to further improve the resolutions both in time and space in the laboratory.

Further work with FTH using a ZP in this configuration has significant challenges when looking for higher resolutions. One possible method to achieve this is to employ a ZP with a smaller outer zone width. By keeping all other aspects of the experiment the same and making the outer zone width 50 nm the resolution could reach 15 nm. This would make the focal distance very short which would make the distance between the ZP and the sample very small.

$$f = \frac{D \Delta r}{\lambda n_{order}} \quad (4.4)$$

with D being the ZP diameter and Δr the outer zone width. For the above example with a ZP with 200 nm outer zone width used in the 3rd order the focal length is $f = 1.7$ mm, while for a ZP with 50 nm outer zone width $f = 0.44$ mm. This may seem trivial but since the ZP are free standing as the ZP become large they can sag or bend out of the plane of the edges of the zone plate. This is depicted in Figure 4.11. This sagging has a significant detrimental effect because as the focus becomes short the Rayleigh length will also be short and this the sag can distort the focus. The distortions to the focus makes the focus waist larger preventing the entire focused beam from passing through the reference hole. As the focal length becomes shorter this effect can have a larger and larger effect. This has been seen in our experiments as shorter ZP focuses were used. One way to correct this issue is to have a ZP that is not free standing. This is a hard trade off since the silicon nitride would cut the photons by 57%. This would require the ZP to run in the 1st order negating the gain by using the 3rd order. Other solution to this issue would be to make use of a ZP that has a smaller outer diameter to reduce the sagging. However, this would reduce the number of photons and the focal length.

This smearing and widening of the focus happens when the ZP is made for one wavelength and order but used for a different wavelength and order. This comes from the way that ZP are made and where the different zones are placed to correct for the aberrations. We found that a ZP made for 46.9 nm and to be used in 1st order also works for 18.9 nm ran in 3rd order.

Another possibility for obtaining better resolution comes from using a shorter wavelength. With using shorter wavelengths the focal length and the Rayleigh become longer. By doing



figures/chap4pic10.png

Figure 4.11: Illustration of zone plate sag and effects on focus.

this the sag would again not be an issue and a higher resolution could be reached. The use of a 50 nm outer zone ZP with a 0.5mm outer diameter that is designed for 3rd order operation at 6.85 nm would give a focal length and Rayleigh length comparable to the ZP used in this experiment. This should result in a resolution of 15 nm to 20 nm and a temporal resolution of 0.7 ps. The challenge is with the development of a Gd 6.85 nm laser with full spatial coherence. As discussed in Chapter 3, a saturated Ni-like Gd laser operating at this wavelength was successfully demonstrated. However, since both a seed and booster amplifiers are needed, it would require more pump energy.

Bibliography

- [1] B. Kaulich, P. Thibault, A. Gianoncelli, and M. Kiskinova, “Transmission and emission x-ray microscopy: Operation modes, contrast mechanisms and applications,” *Journal of Physics: Condensed Matter*, vol. 23, no. 8, p. 083 002, Feb. 2011. DOI: 10.1088/0953-8984/23/8/083002.
- [2] A. Sakdinawat and D. Attwood, “Nanoscale x-ray imaging,” *Nature Photonics*, vol. 4, 840 EP -, Nov. 2010, Review Article. [Online]. Available: <https://doi.org/10.1038/nphoton.2010.267>.
- [3] D. Attwood, *Soft X-Rays and Extreme Ultraviolet Radiation: Principles and Applications*, 1st. New York, NY, USA: Cambridge University Press, 2007.
- [4] M. P. Benk, K. A. Goldberg, A. Wojdyla, C. N. Anderson, F. Salmassi, P. P. Naulleau, and M. Kocsis, “Demonstration of 22-nm half pitch resolution on the sharp euv microscope,” *Journal of Vacuum Science & Technology B*, vol. 33, no. 6, 06FE01, 2015. DOI: 10.1116/1.4929509. eprint: <https://doi.org/10.1116/1.4929509>. [Online]. Available: <https://doi.org/10.1116/1.4929509>.
- [5] W. Chao, B. D. Harteneck, J. A. Liddle, E. H. Anderson, and D. T. Attwood, “Soft x-ray microscopy at a spatial resolution better than 15 nm,” *Nature*, vol. 435, no. 7046, pp. 1210–1213, 2005, ISSN: 1476-4687. DOI: 10.1038/nature03719. [Online]. Available: <https://doi.org/10.1038/nature03719>.
- [6] W. Chao, J. Kim, S. Rekawa, P. Fischer, and E. H. Anderson, “Demonstration of 12 nm resolution fresnel zone plate lens based soft x-ray microscopy,” *Opt. Express*, vol. 17, no. 20, pp. 17 669–17 677, Sep. 2009. DOI: 10.1364/OE.17.017669. [Online]. Available: <http://www.opticsexpress.org/abstract.cfm?URI=oe-17-20-17669>.
- [7] J. Miao, T. Ishikawa, I. K. Robinson, and M. M. Murnane, “Beyond crystallography: Diffractive imaging using coherent x-ray light sources,” *Science*, vol. 348, no. 6234, pp. 530–535,

- 2015, ISSN: 0036-8075. DOI: 10.1126/science.aaa1394. eprint: <https://science.sciencemag.org/content/348/6234/530.full.pdf>. [Online]. Available: <https://science.sciencemag.org/content/348/6234/530>.
- [8] J. Miao, D. Sayre, and H. N. Chapman, "Phase retrieval from the magnitude of the fourier transforms of nonperiodic objects," *J. Opt. Soc. Am. A*, vol. 15, no. 6, pp. 1662–1669, Jun. 1998. DOI: 10.1364/JOSAA.15.001662. [Online]. Available: <http://josaa.osa.org/abstract.cfm?URI=josaa-15-6-1662>.
- [9] E. B. Malm, N. C. Monserud, P. W. Wachulak, H. Xu, G. Balakrishnan, W. Chao, E. Anderson, and M. C. Marconi, "Time resolved extreme ultraviolet fourier transform holography," in *2013 IEEE Photonics Conference*, Sep. 2013, pp. 604–605. DOI: 10.1109/IPCon.2013.6656439.
- [10] D. A. Shapiro, Y.-S. Yu, T. Tyliczszak, J. Cabana, R. Celestre, W. Chao, K. Kaznatcheev, A. L. D. Kilcoyne, F. Maia, S. Marchesini, Y. S. Meng, T. Warwick, L. L. Yang, and H. A. Padmore, "Chemical composition mapping with nanometre resolution by soft x-ray microscopy," *Nature Photonics*, vol. 8, 765 EP -, Sep. 2014. [Online]. Available: <https://doi.org/10.1038/nphoton.2014.207>.
- [11] R. Xu, H. Jiang, C. Song, J. A. Rodriguez, Z. Huang, C.-C. Chen, D. Nam, J. Park, M. Gallagher-Jones, S. Kim, S. Kim, A. Suzuki, Y. Takayama, T. Oroguchi, Y. Takahashi, J. Fan, Y. Zou, T. Hatsui, Y. Inubushi, T. Kameshima, K. Yonekura, K. Tono, T. Togashi, T. Sato, M. Yamamoto, M. Nakasako, M. Yabashi, T. Ishikawa, and J. Miao, "Single-shot three-dimensional structure determination of nanocrystals with femtosecond x-ray free-electron laser pulses," *Nature Communications*, vol. 5, 4061 EP -, Jun. 2014, Article. [Online]. Available: <https://doi.org/10.1038/ncomms5061>.
- [12] M. Holler, M. Guizar-Sicairos, E. H. R. Tsai, R. Dinapoli, E. Müller, O. Bunk, J. Raabe, and G. Aeppli, "High-resolution non-destructive three-dimensional imaging of integrated

- circuits,” *Nature*, vol. 543, 402 EP -, Mar. 2017. [Online]. Available: <https://doi.org/10.1038/nature21698>.
- [13] H. Jiang, C. Song, C.-C. Chen, R. Xu, K. S. Raines, B. P. Fahimian, C.-H. Lu, T.-K. Lee, A. Nakashima, J. Urano, T. Ishikawa, F. Tamanoi, and J. Miao, “Quantitative 3d imaging of whole, unstained cells by using x-ray diffraction microscopy,” *Proceedings of the National Academy of Sciences*, vol. 107, no. 25, pp. 11 234–11 239, 2010, ISSN: 0027-8424. DOI: 10.1073/pnas.1000156107. eprint: <https://www.pnas.org/content/107/25/11234.full.pdf>. [Online]. Available: <https://www.pnas.org/content/107/25/11234>.
- [14] G. K. Tadesse, R. Klas, S. Demmler, S. Hädrich, I. Wahyutama, M. Steinert, C. Spielmann, M. Zürch, T. Pertsch, A. Tünnermann, J. Limpert, and J. Rothhardt, “High speed and high resolution table-top nanoscale imaging,” *Opt. Lett.*, vol. 41, no. 22, pp. 5170–5173, Nov. 2016. DOI: 10.1364/OL.41.005170. [Online]. Available: <http://ol.osa.org/abstract.cfm?URI=ol-41-22-5170>.
- [15] D. F. Gardner, M. Tanksalvala, E. R. Shanblatt, X. Zhang, B. R. Galloway, C. L. Porter, R. Karl Jr, C. Bevis, D. E. Adams, H. C. Kapteyn, M. M. Murnane, and G. F. Mancini, “Sub-wavelength coherent imaging of periodic samples using a 13.5 nm tabletop high-harmonic light source,” *Nature Photonics*, vol. 11, 259 EP -, Mar. 2017, Article. [Online]. Available: <https://doi.org/10.1038/nphoton.2017.33>.
- [16] M. E. Siemens, Q. Li, R. Yang, K. A. Nelson, E. H. Anderson, M. M. Murnane, and H. C. Kapteyn, “Quasi-ballistic thermal transport from nanoscale interfaces observed using ultra-fast coherent soft x-ray beams,” *Nature Materials*, vol. 9, 26 EP -, Nov. 2009. [Online]. Available: <https://doi.org/10.1038/nmat2568>.
- [17] C. von Korff Schmising, B. Pfau, M. Schneider, C. M. Günther, M. Giovannella, J. Perron, B. Vodungbo, L. Müller, F. Capotondi, E. Pedersoli, N. Mahne, J. Lüning, and S. Eisebitt, “Imaging ultrafast demagnetization dynamics after a spatially localized optical excitation,”

- Phys. Rev. Lett.*, vol. 112, p. 217 203, 21 May 2014. DOI: 10.1103/PhysRevLett.112.217203. [Online]. Available: <https://link.aps.org/doi/10.1103/PhysRevLett.112.217203>.
- [18] I. McNulty, J. Kirz, C. Jacobsen, E. H. Anderson, M. R. Howells, and D. P. Kern, “High-resolution imaging by fourier transform x-ray holography,” *Science*, vol. 256, no. 5059, pp. 1009–1012, 1992, ISSN: 0036-8075. DOI: 10.1126/science.256.5059.1009. eprint: <https://science.sciencemag.org/content/256/5059/1009.full.pdf>. [Online]. Available: <https://science.sciencemag.org/content/256/5059/1009>.
- [19] W. F. Schlotter, J. Lüning, R. Rick, K. Chen, A. Scherz, S. Eisebitt, C. M. Günther, W. Eberhardt, O. Hellwig, and J. Stöhr, “Extended field of view soft x-ray fourier transform holography: Toward imaging ultrafast evolution in a single shot,” *Opt. Lett.*, vol. 32, no. 21, pp. 3110–3112, Nov. 2007. DOI: 10.1364/OL.32.003110. [Online]. Available: <http://ol.osa.org/abstract.cfm?URI=ol-32-21-3110>.
- [20] S. Eisebitt, J. Lüning, W. F. Schlotter, M. Lörger, O. Hellwig, W. Eberhardt, and J. Stöhr, “Lensless imaging of magnetic nanostructures by x-ray spectro-holography,” *Nature*, vol. . 432, no. 7019, pp. 885–888, 2004, ISSN: 1476-4687. DOI: 10.1038/nature03139. [Online]. Available: <https://doi.org/10.1038/nature03139>.
- [21] S. Marchesini, S. Boutet, A. E. Sakdinawat, M. J. Bogan, S. Bajt, A. Barty, H. N. Chapman, M. Frank, S. P. Hau-Riege, A. Szöke, C. Cui, D. A. Shapiro, M. R. Howells, J. C. H. Spence, J. W. Shaevitz, J. Y. Lee, J. Hajdu, and M. M. Seibert, “Massively parallel x-ray holography,” *Nature Photonics*, vol. 2, 560 EP -, Aug. 2008. [Online]. Available: <https://doi.org/10.1038/nphoton.2008.154>.
- [22] S. Schaffert, B. Pfau, J. Geilhufe, C. M. Gffdfddnther, M. Schneider, C. von Korff Schmis- ing, and S. Eisebitt, “High-resolution magnetic-domain imaging by fourier transform holography at 21 nm wavelength,” *New Journal of Physics*, vol. 15, no. 9, p. 093 042, Sep. 2013. DOI: 10.1088/1367-2630/15/9/093042.

- [23] R. L. Sandberg, D. A. Raymondson, C. La-o-vorakiat, A. Paul, K. S. Raines, J. Miao, M. M. Murnane, H. C. Kapteyn, and W. F. Schlotter, “Tabletop soft-x-ray fourier transform holography with 50 nm resolution,” *Opt. Lett.*, vol. 34, no. 11, pp. 1618–1620, Jun. 2009. DOI: 10.1364/OL.34.001618. [Online]. Available: <http://ol.osa.org/abstract.cfm?URI=ol-34-11-1618>.
- [24] G. K. Tadesse, W. Eschen, R. Klas, V. Hilbert, D. Schelle, A. Nathanael, M. Zilk, M. Steinert, F. Schrepel, T. Pertsch, A. Tünnermann, J. Limpert, and J. Rothhardt, “High resolution xuv fourier transform holography on a table top,” *Scientific Reports*, vol. 8, no. 1, p. 8677, 2018, ISSN: 2045-2322. DOI: 10.1038/s41598-018-27030-y. [Online]. Available: <https://doi.org/10.1038/s41598-018-27030-y>.
- [25] H. T. Kim, I. J. Kim, C. Kim, T. M. Jeong, T. J. Yu, S. K. Lee, J. Sung, J. W. Yoon, H. Yun, S. C. Jeon, I. W. Choi, and J. Lee, “Single-shot nanometer-scale holographic imaging with laser-driven x-ray laser,” *Applied Physics Letters*, vol. 98, pp. 121 105–121 105, Mar. 2011. DOI: 10.1063/1.3560466.
- [26] M. Sacchi, H. Popescu, N. Jaouen, M. Tortarolo, F. Fortuna, R. Delaunay, and C. Spezzani, “Magnetic imaging by fourier transform holography using linearly polarized x-rays,” *Optics express*, vol. 20, pp. 9769–76, Apr. 2012. DOI: 10.1364/OE.20.009769.
- [27] S. Hädrich, J. Rothhardt, M. Krebs, S. Demmler, A. Klenke, A. Tünnermann, and J. Limpert, “Single-pass high harmonic generation at high repetition rate and photon flux,” *Journal of Physics B: Atomic, Molecular and Optical Physics*, vol. 49, no. 17, p. 172 002, Aug. 2016. DOI: 10.1088/0953-4075/49/17/172002.
- [28] J. Rothhardt, S. Hädrich, A. Klenke, S. Demmler, A. Hoffmann, T. Gotschall, T. Eidam, M. Krebs, J. Limpert, and A. Tünnermann, “53 w average power few-cycle fiber laser system generating soft x rays up to the water window,” *Opt. Lett.*, vol. 39, no. 17, pp. 5224–5227, Sep. 2014. DOI: 10.1364/OL.39.005224. [Online]. Available: <http://ol.osa.org/abstract.cfm?URI=ol-39-17-5224>.

- [29] R. Klas, S. Demmler, M. Tschernajew, S. Hädrich, Y. Shamir, A. Tünnermann, J. Rothhardt, and J. Limpert, “Table-top milliwatt-class extreme ultraviolet high harmonic light source,” *Optica*, vol. 3, no. 11, pp. 1167–1170, Nov. 2016. DOI: 10.1364/OPTICA.3.001167. [Online]. Available: <http://www.osapublishing.org/optica/abstract.cfm?URI=optica-3-11-1167>.
- [30] G. Vaschenko, C. Brewer, F. Brizuela, Y. Wang, M. A. Larotonda, B. M. Luther, M. C. Marconi, J. J. Rocca, C. S. Menoni, E. H. Anderson, W. Chao, B. D. Harteneck, J. A. Liddle, Y. Liu, and D. T. Attwood, “Sub-38 nm resolution tabletop microscopy with 13 nm wavelength laser light,” *Opt. Lett.*, vol. 31, no. 9, pp. 1214–1216, May 2006. DOI: 10.1364/OL.31.001214. [Online]. Available: <http://ol.osa.org/abstract.cfm?URI=ol-31-9-1214>.
- [31] P. W. Wachulak, M. C. Marconi, R. A. Bartels, C. S. Menoni, and J. J. Rocca, “Soft x-ray laser holography with wavelength resolution,” *J. Opt. Soc. Am. B*, vol. 25, no. 11, pp. 1811–1814, Nov. 2008. DOI: 10.1364/JOSAB.25.001811. [Online]. Available: <http://josab.osa.org/abstract.cfm?URI=josab-25-11-1811>.
- [32] R. A. London, M. Strauss, and M. D. Rosen, “Modal analysis of x-ray laser coherence,” *Phys. Rev. Lett.*, vol. 65, pp. 563–566, 5 Jul. 1990. DOI: 10.1103/PhysRevLett.65.563. [Online]. Available: <https://link.aps.org/doi/10.1103/PhysRevLett.65.563>.
- [33] C. Lewis, D. Neely, D. O’Neill, J. Uhomobhi, M. Key, Y. Al Hadithi, G. Tallents, and S. Ramsden, “An injector/amplifier double target configuration for the ne-like ge x-ray laser scheme,” *Optics Communications*, vol. 91, pp. 71–76, Jul. 1992. DOI: 10.1016/0030-4018(92)90103-X.
- [34] R. E. Burge, G. E. Slark, M. T. Browne, X.-C. Yuan, P. Charalambous, X.-H. Cheng, C. L. S. Lewis, A. MacPhee, and D. Neely, “Spatial coherence of x-ray laser emission from neonlike germanium after prepulse,” *J. Opt. Soc. Am. B*, vol. 14, no. 10, pp. 2742–2751, Oct. 1997. DOI: 10.1364/JOSAB.14.002742. [Online]. Available: <http://josab.osa.org/abstract.cfm?URI=josab-14-10-2742>.

- [35] H. Daido, S. Sebban, N. Sakaya, Y. Tohyama, T. Norimatsu, K. Mima, Y. Kato, S. Wang, Y. Gu, G. Huang, H. Tang, K. Murai, R. Butzbach, I. Uschmann, M. Vollbrecht, and E. Förster, “Experimental characterization of short-wavelength ni-like soft-x-ray lasing toward the water window,” *J. Opt. Soc. Am. B*, vol. 16, no. 12, pp. 2295–2299, Dec. 1999. DOI: 10.1364/JOSAB.16.002295. [Online]. Available: <http://josab.osa.org/abstract.cfm?URI=josab-16-12-2295>.
- [36] G. Cairns, C. L. S. Lewis, A. G. MacPhee, D. Neely, M. Holden, J. Krishnan, G. J. Tallents, M. H. Key, P. N. Norreys, C. G. Smith, J. Zhang, P. B. Holden, G. J. Pert, J. Plowes, and S. A. Ramsden, “Preliminary studies of radiation coupling between remote soft x-ray laser amplifiers,” *Applied Physics B*, vol. 58, no. 1, pp. 51–56, Jan. 1994, ISSN: 1432-0649. DOI: 10.1007/BF01081713. [Online]. Available: <https://doi.org/10.1007/BF01081713>.
- [37] R. Kodama, D. Neely, Y. Kato, H. Daido, K. Murai, G. Yuan, A. MacPhee, and C. L. S. Lewis, “Generation of small-divergence soft x-ray laser by plasma waveguiding with a curved target,” *Phys. Rev. Lett.*, vol. 73, pp. 3215–3218, 24 Dec. 1994. DOI: 10.1103/PhysRevLett.73.3215. [Online]. Available: <https://link.aps.org/doi/10.1103/PhysRevLett.73.3215>.
- [38] M. Nishikino, M. Tanaka, K. Nagashima, M. Kishimoto, M. Kado, T. Kawachi, K. Sukegawa, Y. Ochi, N. Hasegawa, and Y. Kato, “Demonstration of a soft-x-ray laser at 13.9 nm with full spatial coherence,” *Phys. Rev. A*, vol. 68, Dec. 2003. DOI: 10.1103/PhysRevA.68.061802.
- [39] M. Born and E. Wolf, *Principles of Optics: Electromagnetic Theory of Propagation, Interference and Diffraction of Light (7th Edition)*, 7th. Cambridge University Press, 1999, ISBN: 0521642221.
- [40] J. Meszaros, “Large area zone plate exposure by fixed beam moving stage lithography,” 2011.
- [41] D. Attwood, *Soft X-Rays and Extreme Ultraviolet Radiation*. Aug. 1999.

Chapter 5

Summary

The work in this dissertation has resulted in the demonstration of a Petawatt-class (0.85 PW) ultrashort pulse laser capable to fire at repetition rates up to 3.3 Hz, the highest repetition rate at which such lasers have operated to date. The high repetition rate is made possible by pumping with high energy Nd:glass slab amplifiers. This Ti:Sapphire laser can be operated in second harmonic mode to produce pulses of ultra-high contrast. This makes it a valuable tool to study the interaction of high intensity laser pulses with solid targets at relativistic intensity. Significant progress was also obtained in the development of high pulse energy compact SXR lasers at sub-7 nm wavelengths as well as an increase in the diversity of SXR laser wavelengths available. The results were obtained by irradiating slab targets of lanthanide elements at grazing incidence. Measurements showed that the trend of optimum grazing incident angle vs atomic number is linear. Gain-saturated table-top SXR lasers were extended down to 6.85 nm by transient excitation of nickel-like ions in a gadolinium plasma using the combination of a pre-pulse and a sub-ps pump laser pulse. Operation at 6.85 nm resulted in a maximum energy per pulse of 1.8 μJ . Using this sub-picosecond optical laser pump also resulted in amplification at wavelengths as short as 5.85 nm. This short wavelength, microjoule pulse energy, picosecond pulse duration and the repetitive operation of these lasers will enable new applications such as sequential imaging of ultrafast nano-scale dynamic phenomena to be realized in a compact set up. A demonstration of single shot holographic imaging over a large field of view was realized. Using a zone plate 200 nm silver nano-wires were imaged with temporal resolution of 5 ps and a spatial resolution of 62 nm. The use of an optimized zone plate would yield single-shot holograms with a resolution better than 20 nm.

Appendix A

RELATED WORK

Previous chapters discuss the development of a Ti:Sapphire laser system as well as gain-saturated table-top repetitive SXR lasers with wavelengths near 7-5 nm with lasing down to 5.85 nm and the creation of holographic images with 62nm resolution and temporal resolution of 5 ps. The work done in this thesis contributed to the development and characterization x-ray pulse generation, micro-scale fusion and electron acceleration. All these results and more are discussed in the following publications and talks:

Efficient picosecond X-ray pulses from plasma in the radiation dominated regime

- R. Hollinger, B. Bargsten, V.N. Shlyaptsev, V. Kaymak, A. Pukhov, M.G. Capeluto, S. Wang, A. Rockwood, Y. Wang, A. Townsend, A. Prieto, J.J. Rocca, "Efficient picosecond X-ray pulses from plasma in the radiation dominated regime", *Optica*, 4, 1344, (2017).

Micro-scale fusion in dense relativistic nanowire array plasmas

- A. Curtis, C. Calvi, J. Tinsley, R. Hollinger, V. Kaymak, A. Pukhov, S.J. Wang, A. Rockwood, Y. Wang, V.N. Shlyaptsev and J.J. Rocca, "Micro-scale fusion in dense relativistic nanowire array plasmas". *Nature Communications*. 9,1077, (2018).

Energy penetration into arrays of aligned nanowires irradiated with relativistic intensities: scaling to terabar pressures

- C. Bargsten, R. Hollinger, M. Gabriela Capeluto, V. Kaymak, A. Pukhov, S. Wang, A. Rockwood, Y. Wang, D. Keiss, R. Tommasini, R. London, J. Park, M. Busquet, M. Klapisch, V. N. Shlyaptsev, J.J. Rocca, " Energy penetration into arrays of aligned nanowires irradiated with relativistic intensities: scaling to terabar pressures", *Science Advances*, 3, e1601558 (2017).

- J. J. Rocca, B. A. Reagan, C. Baumgarten, M. Pedicone, R. Hollinger, M. G. Capeluto, C. Barnngsten, V. N. Shlyaptsev, V. Kaymak, A. Pukhov, Y. Wang, S. Wang, A. Rockwood, M. Berrill and C. S. Menoni, "High Repetition Rate Soft X-Ray Lasers and Bright Table-top X-Ray Plasma Sources from Nanostructured Targets," in High-Brightness Sources and Light-Driven Interactions, OSA technical Digest (online) (Optical Society of America, 2016), paper ES3A.4.

High Power Ultrashort Pulse Lasers to Pump Plasma-Based Soft X-ray Lasers

- S. Wang, C. Baumgarten, Y. Wang, B. A. Reagan, A. Rockwood, H. Wang, L. Yin, K. A. Wernsing, H. Bravo, B. Luther, C. S. Menoni, J. J. Rocca "High Power Ultrashort Pulse Lasers to Pump Plasma-Based Soft X-ray Lasers," in IEEE Journal of Selected Topics in Quantum Electronics, pp. 1-1, 2019,

Enhanced electron acceleration in aligned nanowire arrays irradiated at highly relativistic intensities

- A. Moreau, R. Hollinger, C. Calvi, S. Wang, Y. Wang, M. G. Capeluto, A. Rockwood, A. Curtis, S. Kasdorf, V. N. Shlyaptsev, V. Kaymak, A. Pukhov and J. J. Rocca, "Enhanced electron acceleration in aligned nanowire arrays irradiated at highly relativistic intensities," Plasma Physics and Controlled Fusion, vol. 62, no. 1, p. 014 013, Nov. 2019. DOI: 10.1088/1361-6587/ab4d0c